

Representation Learning for Extrapolation in Perturbation Modeling

Julius von Kügelgen¹ Jakob Ketterer² Xinwei Shen³ Nicolai Meinshausen¹ Jonas Peters¹

Abstract

We consider the problem of modeling the effects of perturbations, such as gene knockdowns or drugs, on measurements, such as single-cell RNA or protein counts. Given data for some perturbations, we aim to predict the distribution of measurements for new combinations of perturbations. To address this challenging extrapolation task, we posit that perturbations act additively in a suitable, unknown embedding space. We formulate the data-generating process as a latent variable model, in which perturbations amount to mean shifts in latent space and can be combined additively. We then prove that, given sufficiently diverse training perturbations, the representation and perturbation effects are identifiable up to orthogonal transformation and use this to characterize the class of unseen perturbations for which we obtain extrapolation guarantees. We establish a link between our model class and shift interventions in linear latent causal models. To estimate the model from data, we propose a new method, the perturbation distribution autoencoder (PDAE), which is trained by maximizing the distributional similarity between true and simulated perturbation distributions. The trained model can then be used to predict previously unseen perturbation distributions. Through simulations, we demonstrate that PDAE can accurately predict the effects of unseen but identifiable perturbations, supporting our theoretical results.

1 Introduction

Due to technological progress, large-scale perturbation data is becoming increasingly abundant across several scientific fields. In single-cell biology, for example, advancements in gene editing, sequencing, and mass spectrometry have led to the collection of vast transcriptomic or proteomic databases for various drug and gene perturbations (Wang et al., 2009;

¹Seminar for Statistics, ETH Zürich, Zürich, Switzerland ²ETH Zürich, Zürich, Switzerland ³University of Washington, Seattle, USA. Correspondence to: <vjulius@ethz.ch>.

Jinek et al., 2012; Dixit et al., 2016; Norman et al., 2019; Zhang et al., 2025). However, the exponential number of possible combinations of perturbations renders exhaustive experimentation prohibitive. Observations are thus typically only available for a subset of perturbations of interest, e.g., some single and double gene knockdowns or certain dosages of drugs. Having models capable of extrapolating to unseen combinations of perturbations, e.g., new multi-gene knockdowns or dosage combinations, would be highly desirable.

Prior work. Several studies advocate for the use of machine learning for biological perturbation modeling (Lopez et al., 2018; 2023; Hugi et al., 2025), often aiming to generalize to new cell types (Lotfollahi et al., 2019; Bunne et al., 2023; Adduri et al., 2025); unseen combinations of perturbations (Lotfollahi et al., 2023; Bereket & Karaletsos, 2023); entirely new perturbations by leveraging the molecular structure of the involved compounds (Yu & Welch, 2022; Hetzel et al., 2022; Qi et al., 2024) or known gene-gene interactions (Roohani et al., 2024; Kamimoto et al., 2023); or combinations thereof (He et al., 2025; Adduri et al., 2025). A common theme is the use of nonlinear representation learning techniques such as autoencoders to embed observations in a latent space, in which the effects of perturbations are assumed to take on a simpler (e.g., additive) form. However, existing studies are purely empirical and lack theoretical underpinning. The capabilities and fundamental limitations of existing methods thus remain poorly understood.

Overview and contributions. In this work, we present theoretically-grounded perspective on perturbation extrapolation. Given the typically unpaired nature of the available non-i.i.d. data—e.g., each cell can only be measured once since the measurement process is destructive—we consider the task of predicting population-level perturbation effects, which we formalize as a distributional regression problem (§ 2). We then postulate a generative model (§ 3) which, similar to prior works, assumes that perturbations act as mean shifts in a suitable latent space, see Fig. 1 for an overview. For the case of a deterministic decoder, we analyse this model class theoretically (§ 4), proving that, under mild assumptions, the latent representation and the relative training perturbation effects are identifiable up to orthogonal transformation if the available environments are sufficiently diverse (Thm. 4.1). This result implies extrapolation guarantees for certain unseen perturbations that can be expressed as

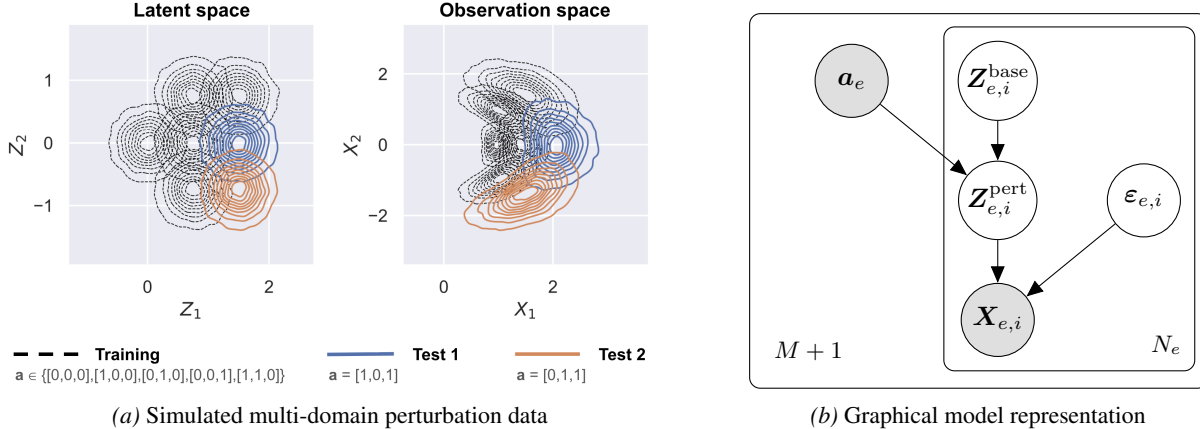


Figure 1. Task description and example following the assumed data generating process. (a) During training, we are given $M = 5$ training data sets in observation space (right, contour plots in grey), each of which is generated under a known combination of $K = 3$ elementary perturbations. The corresponding (training) perturbation labels \mathbf{a}_e are shown below the plots. During testing, we are given a new perturbation label and the task is to predict the corresponding distribution in observation space (right, blue and orange). We tackle this task by assuming that the effect of perturbations is linear additive in a suitable latent space (left). Both plots show kernel density estimates of the distributions. (b) For each experiment or environment $e \in [M]_0$, the corresponding dataset comprises a perturbation label \mathbf{a}_e and N_e observations $\mathbf{x}_{e,i}$. Perturbations are assumed to act as mean-shifts on a latent basal state, $\mathbf{z}_{e,i}^{\text{pert}} = \mathbf{z}_{e,i}^{\text{base}} + \mathbf{W}\mathbf{a}_e$ for an unknown perturbation matrix \mathbf{W} . An (unknown) stochastic nonlinear decoder with noise $\boldsymbol{\varepsilon}_{e,i}$ then yields the observed $\mathbf{x}_{e,i} = \mathbf{f}(\mathbf{z}_{e,i}^{\text{pert}}, \boldsymbol{\varepsilon}_{e,i})$. In the example in (a), \mathbf{f} is constant in its second argument. Shaded and white nodes indicate observed and unobserved/latent variables, respectively.

linear combinations of training perturbations (Thm. 4.7). By considering shift interventions in linear structural equation models, we establish a connection between our model class and causal representation learning (Prop. 4.9). Based on our theoretical results, we then propose an autoencoder-based estimation method (§ 5) which uses the energy score (Gneiting & Raftery, 2007) to assess distributional similarity between predicted and ground-truth perturbation data. In simulations (§ 7), this approach compares favourably to relevant baselines in terms of mean prediction and distributional fit.

Notation. We write scalars as a , column-vectors as \mathbf{a} , and matrices as \mathbf{A} . We use uppercase for random variables and lowercase for their realizations. The pushforward of a distribution \mathbb{P} by a measurable function f is denoted by $f_{\#}\mathbb{P}$. The Euclidean (ℓ_2) norm is denoted by $\|\cdot\|$. For $n \in \mathbb{N}_{\geq 1}$, we use the shorthands $[n] := \{1, \dots, n\}$ and $[n]_0 := [n] \cup \{0\}$.

2 Distributional perturbation extrapolation

Observables. Let $\mathbf{x} \in \mathbb{R}^{d_x}$ be an *observation* (e.g., omics data) that is obtained under one of several possible experimental conditions, and let \mathbf{X} be the corresponding random vector. We model these conditions as combinations of K elementary perturbations, each of which we assume can be encoded by a real number. Further, let $\mathbf{a} \in \mathbb{R}^K$ be a vector of *perturbation labels* that indicates if, or how much of, each perturbation was applied before collecting \mathbf{x} .

Example 2.1 (Gene perturbations). For data arising from gene knockouts, a perturbation can be represented by a binary $\mathbf{a} \in \{0, 1\}^K$, where K denotes the number of potential

targets and $a_k = 1$ if and only if target k was subject to a knockout experiment. For example, $\mathbf{a} = (1, 0, 1, 0, 0)$ indicates a multi-gene knockout on targets one and three.

Example 2.2 (Drug perturbations). For data arising from applying varying amounts of K different drugs, perturbations can be represented by continuous, non-negative labels $\mathbf{a} \in \mathbb{R}_+^K$, where a_k indicates the (relative or absolute) amount of drug k that was administered.

Data. We have access to $M + 1$ experimental datasets $\mathcal{D}_0, \mathcal{D}_1, \dots, \mathcal{D}_M$, each comprising a sample of N_e observations \mathbf{x} and a perturbation label \mathbf{a} , i.e., for all experiments or environments $e \in [M]_0$,

$$\mathcal{D}_e = ((\mathbf{x}_{e,i})_{i=1}^{N_e}, \mathbf{a}_e). \quad (2.1)$$

For all $e \in [M]_0$, we assume that $\mathbf{x}_{e,1}, \dots, \mathbf{x}_{e,N_e}$ are i.i.d. realizations from some underlying distribution $\mathbb{P}_{\mathbf{X}|\mathbf{a}_e}$.

Task. Given data in the form of (2.1), we aim to predict the effects of new perturbations $\mathbf{a}_{\text{test}} \notin \{\mathbf{a}_0, \mathbf{a}_1, \dots, \mathbf{a}_M\}$ without observing any data from this condition (“zero-shot”). In particular, we are interested in the distribution over observations resulting from \mathbf{a}_{test} . That is, we aim to leverage the training domains (2.1) to learn a map

$$\mathbf{a} \mapsto \mathbb{P}_{\mathbf{X}|\mathbf{a}}, \quad (2.2)$$

which extrapolates beyond the training support of \mathbf{a} , i.e., the predictions should remain reliable for new inputs \mathbf{a}_{test} .

Distributional vs mean prediction. Since (2.2) targets the full conditional distribution—rather than, say, the condi-

tional mean $\mathbb{E}[\mathbf{X}|\mathbf{a}]$ —it constitutes a (multi-variate) distributional regression task (Koenker & Bassett Jr, 1978), a.k.a. probabilistic forecasting (Gneiting & Raftery, 2007) or conditional generative modeling (Sohn et al., 2015). Therefore, we refer to the problem setting addressed in this paper as *distributional* perturbation extrapolation.

On extrapolation. Formally, extrapolation means that the value of the function (2.2) at \mathbf{a}_{test} is determined by its values on the training support $\{\mathbf{a}_0, \mathbf{a}_1, \dots, \mathbf{a}_M\}$. Intuitively, for this to be feasible without imposing very restrictive assumptions on the form of the mapping in (2.2), \mathbf{a}_{test} should be somehow related to the training perturbations \mathbf{a}_e . For example, given data resulting from individual perturbations, predict the effects of combinations thereof. This type of extrapolation to new combinations of inputs is also called compositional generalization (Lake et al., 2017; Goyal & Bengio, 2022). It is known to be challenging (Schott et al., 2022; Montero et al., 2021; 2022) and requires assumptions that sufficiently constrain the model class (Wiedemer et al., 2024a,b; Lachapelle et al., 2023; Brady et al., 2023; 2025; Dong & Ma, 2022; Lippel & Stachenfeld, 2024).

3 Perturbations as mean shifts in latent space

We now specify a generative process for the observed data in (2.1). In so doing, we aim to strike a balance between imposing sufficient structure on (2.2) to facilitate extrapolation, while remaining flexible enough to model the complicated, nonlinear effects which perturbations may have on the distribution of observations. Similar to other approaches (e.g., Lotfollahi et al., 2023; Bereket & Karaletsos, 2023), we model the effect of perturbations as mean shifts in a latent space with perturbation-relevant latent variables $\mathbf{z} \in \mathbb{R}^{d_z}$, which are related to the observations \mathbf{x} via a nonlinear (stochastic) *mixing function* or *generator* \mathbf{f} . The full generative process amounts to a hierarchical latent variable model, which additionally contains *noise variables* ε that capture other variation underlying the observations \mathbf{x} , and which is represented as a graphical model in Fig. 1b. Specifically, we posit for all $e \in [M]_0 \cup \{\text{test}\}$ and all $i \in [N_e]$:

$$\mathbf{Z}_{e,i}^{\text{base}} \sim \mathbb{P}_{\mathbf{Z}}, \quad \mathbf{Z}_{e,i}^{\text{pert}} := \mathbf{Z}_{e,i}^{\text{base}} + \mathbf{W}\mathbf{a}_e, \quad (3.1)$$

$$\varepsilon_{e,i} \sim \mathbb{Q}_{\varepsilon}, \quad \mathbf{X}_{e,i} := \mathbf{f}(\mathbf{Z}_{e,i}^{\text{pert}}, \varepsilon_{e,i}), \quad (3.2)$$

where $(\mathbf{Z}_{e,i}^{\text{base}})_{e \in [M]_0, i \in [N_e]}$ are i.i.d. according to $\mathbb{P}_{\mathbf{Z}}$, and $(\varepsilon_{e,i})_{e \in [M]_0, i \in [N_e]}$ are i.i.d. according to \mathbb{Q}_{ε} and jointly independent of $(\mathbf{Z}_{e,i}^{\text{base}})_{e \in [M]_0, i \in [N_e]}$.

The *basal state* \mathbf{Z}^{base} in (3.1) describes the unperturbed state of latent variables, which can, in principle, be affected by perturbations, and is distributed according to a base distribution $\mathbb{P}_{\mathbf{Z}}$. The *perturbation matrix* $\mathbf{W} \in \mathbb{R}^{d_z \times K}$ captures the effect of the K elementary perturbations encoded in \mathbf{a} on the latents and turns \mathbf{Z}^{base} into *perturbed latents* \mathbf{Z}^{pert} .

Since the same perturbation \mathbf{a}_e is applied for all $i \in [N_e]$, all within-dataset variability in \mathbf{Z}^{pert} is due to $\mathbb{P}_{\mathbf{Z}}$. The noise variables $\varepsilon \in \mathbb{R}^{d_{\varepsilon}}$ in (3.2) capture all other variation in the observed data that is unaffected by perturbations. W.l.o.g., we assume that it is distributed according to a fixed, uninformative distribution \mathbb{Q}_{ε} such as a standard isotropic Gaussian. The noise serves as an additional input to the (stochastic) mixing function or generator $\mathbf{f} : \mathbb{R}^{d_z} \times \mathbb{R}^{d_{\varepsilon}} \rightarrow \mathbb{R}^{d_x}$, which produces observations for the perturbed latent. This implicit generative model can capture any conditional distribution $\mathbb{P}_{\mathbf{X}|\mathbf{Z}=\mathbf{z}}$ (e.g., Peters et al., 2017, Prop. 7.1) and is more flexible than relying on parametric assumptions, such as a Gaussian (Lotfollahi et al., 2023) or negative Binomial (Bereket & Karaletsos, 2023; Lopez et al., 2018; 2023) likelihood parametrised by a deterministic decoder.

For a given e and \mathbf{a}_e , the generative process in (3.1) and (3.2) induces a distribution over observations \mathbf{x} , which we denote by \mathbb{P}_e or $\mathbb{P}_{\mathbf{X}|\mathbf{a}_e}$, defined as the push-forward of $\mathbb{P}_{\mathbf{Z}}$ and \mathbb{Q}_{ε} through (3.1) and (3.2), such that for all $e \in [M]_0$:

$$(\mathbf{X}_{e,i})_{i \in [N_e]} \stackrel{\text{i.i.d.}}{\sim} \mathbb{P}_e. \quad (3.3)$$

4 Theoretical results

We now present our theoretical analysis for the model class from § 3. Here, we assume that the decoder is deterministic, so that we can write $\mathbf{f} : \mathbb{R}^{d_z} \rightarrow \mathbb{R}^{d_x}$, see Remark 4.6 for further discussion. All proofs are provided in § A.

4.1 Identifiability

We first study identifiability, i.e., under which assumptions and up to which ambiguities certain parts of the postulated generative process can be provably recovered given access to the full distributions. As established by the following results, our model class is identifiable up to orthogonal transformation, provided that the training perturbations are sufficiently diverse, the dimension of the latent space is known, and some additional technical assumptions hold.

Theorem 4.1 (Identifiability up to orthogonal transformation). *For $M \in \mathbb{Z}_{\geq 0}$, let $\mathbf{a}_0, \dots, \mathbf{a}_M \in \mathbb{R}^K$ be $M+1$ perturbation labels. Let $\mathbf{f}, \tilde{\mathbf{f}} : \mathbb{R}^{d_z} \rightarrow \mathbb{R}^{d_x}$, $\mathbf{W}, \tilde{\mathbf{W}} \in \mathbb{R}^{d_z \times K}$, and $\mathbb{P}, \tilde{\mathbb{P}}$ be distributions on \mathbb{R}^{d_z} such that the models $(\mathbf{f}, \mathbf{W}, \mathbb{P})$ and $(\tilde{\mathbf{f}}, \tilde{\mathbf{W}}, \tilde{\mathbb{P}})$ induce the same observed distributions, i.e., for all $e \in [M]_0$:*

$$\mathbf{f}(\mathbf{Z} + \mathbf{W}\mathbf{a}_e) \stackrel{d}{=} \tilde{\mathbf{f}}(\tilde{\mathbf{Z}} + \tilde{\mathbf{W}}\mathbf{a}_e), \quad (4.1)$$

with $\mathbf{Z} \sim \mathbb{P}$ and $\tilde{\mathbf{Z}} \sim \tilde{\mathbb{P}}$ independent. Assume further that:

- (i) **[invertibility]** \mathbf{f} and $\tilde{\mathbf{f}}$ are C^2 -diffeomorphisms onto their respective images;
- (ii) **[Gaussianity]** \mathbf{Z} and $\tilde{\mathbf{Z}}$ are standard isotropic multivariate Gaussians with means chosen such that the latent

distributions in domain $e = 0$ are centered at the origin, i.e., $\mathbb{P} = \mathcal{N}(-W\mathbf{a}_0, \mathbf{I})$ and $\widetilde{\mathbb{P}} = \mathcal{N}(-\widetilde{W}\mathbf{a}_0, \mathbf{I})$;

(iii) [sufficient diversity] the matrix $\widetilde{W}\mathbf{A} \in \mathbb{R}^{d_Z \times M}$, where $\mathbf{A} \in \mathbb{R}^{K \times M}$ is the matrix with columns $(\mathbf{a}_1 - \mathbf{a}_0), \dots, (\mathbf{a}_M - \mathbf{a}_0)$, has full row rank, i.e., $\text{rank}(\widetilde{W}\mathbf{A}) = d_Z$, or the same holds for $W\mathbf{A}$.

Then the latent representation and the effects of the observed perturbation combinations relative to \mathbf{a}_0 (as captured by $W\mathbf{A}$) are identifiable up to orthogonal transformation, i.e., there is an orthogonal matrix $\mathbf{O} \in O(d_Z)$ such that

$$\forall z \in \mathbb{R}^{d_Z} : \quad \widetilde{\mathbf{f}}^{-1} \circ \mathbf{f}(z) = \mathbf{O}z, \quad (4.2)$$

$$\widetilde{W}\mathbf{A} = \mathbf{O}W\mathbf{A}. \quad (4.3)$$

Corollary 4.2. If, in addition to the assumptions of Thm. 4.1, $\mathbf{A} \in \mathbb{R}^{K \times M}$ has full row rank (i.e., $\text{rank}(\mathbf{A}) = K \leq M$), then the perturbation matrix W is identifiable up to orthogonal transformation, i.e., $\widetilde{W} = \mathbf{O}W$, where $\mathbf{O} \in O(d_Z)$ is an orthogonal matrix.

Discussion. Thm. 4.1 can be interpreted as follows. Fix a set of perturbation labels $(\mathbf{a}_0, \dots, \mathbf{a}_M)$ and a data generating process parametrised by (\mathbf{f}, W) . Then, for all \widetilde{W} such that (4.3) holds for some $\mathbf{O} \in O(d_Z)$, there exists a unique $\widetilde{\mathbf{f}}$, characterized by (4.2), such that the model parametrised by $(\widetilde{\mathbf{f}}, \widetilde{W})$ gives rise to the same observed distributions of \mathbf{X}_e . At the same time, any $(\widetilde{\mathbf{f}}, \widetilde{W})$ for which this holds for all $e \in [M]_0$ is of that form. In other words, the mixing function \mathbf{f} and the relative shift matrix $W\mathbf{A}$ are identifiable up to orthogonal transformation—provided that the observed training perturbation conditions are sufficiently diverse, as formalised by assumption (iii).

Remark 4.3 (Choice of base distribution). The choice of means and covariances in assumption (ii) of Thm. 4.1 serves to eliminate inherent ambiguities of the model class due to overparametrisation. As shown by Lemma A.1, this comes w.l.o.g., in the sense that any model with $\mathbb{P} = \mathcal{N}(\boldsymbol{\mu}, \boldsymbol{\Sigma})$ can be reparametrised to take the form in assumption (ii).

Remark 4.4 (Sufficient diversity). The matrix product $W\mathbf{A} \in \mathbb{R}^{d_Z \times M}$ captures the relative effects of the observed perturbations since $(W\mathbf{A})_{je}$ corresponds to the shift in the j^{th} latent Z_j resulting from \mathbf{a}_e , relative to a reference condition \mathbf{a}_0 . Moreover, assumption (iii) of Thm. 4.1 implies

$$\min \{ \text{rank}(\widetilde{W}), \text{rank}(\mathbf{A}) \} \geq \text{rank}(\widetilde{W}\mathbf{A}) = d_Z. \quad (4.4)$$

Hence, sufficient diversity requires at least d_Z elementary perturbations whose associated shift vectors $\mathbf{w}_k \in \mathbb{R}^{d_Z}$ are linearly independent, and we must observe at least d_Z perturbation conditions \mathbf{a}_e other than \mathbf{a}_0 such that the relative perturbation vectors $(\mathbf{a}_e - \mathbf{a}_0) \in \mathbb{R}^K$ are linearly independent.

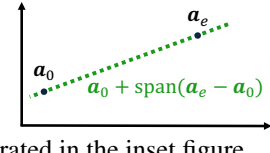
Remark 4.5 (Choice of reference). The choice of reference environment is arbitrary. Here, we choose $e = 0$ as reference without loss of generality. Intuitively, if a perturbation

is always present (e.g., $a_{e,1} = 1$ for all e), then its effects cannot be discerned from the basal state. Therefore, only the effects of the relative perturbations $(\mathbf{a}_e - \mathbf{a}_0)$ can be recovered. In practice, we often have access to an unperturbed, purely observational control condition with $\mathbf{a}_0 = 0$.

Remark 4.6 (Deterministic vs noisy mixing.). The mixing function \mathbf{f} in Thm. 4.1 is assumed deterministic, i.e., does not take noise ε as input, cf. (3.2). In principle, this does not pose a restriction since noise can be appended to \mathbf{z}^{pert} as additional dimensions that are not influenced by perturbations. However, this increases d_Z and makes it harder to satisfy sufficient diversity (see Remark 4.4). Alternatively, the additive noise setting, $\mathbf{X} = \mathbf{f}(\mathbf{Z}) + \varepsilon$, can be reduced to the noiseless case (Khemakhem et al., 2020).

4.2 From identifiability to extrapolation

Since we aim to make distributional predictions for new perturbations \mathbf{a}_{test} , identifiability is only of intermediary interest. The following result highlights the usefulness of identifiability up to orthogonal transformation established in Thm. 4.1 for extrapolation. It allows us to uniquely predict the observable effects of certain unseen perturbations—those which can be expressed as linear combinations of the observed perturbations, as illustrated in the inset figure.



Theorem 4.7 (Extrapolation to span of relative perturbations). Under the same setting and assumptions as in Thm. 4.1, let $\mathbf{a}_{\text{test}} \in \mathbb{R}^K$ be an unseen perturbation s.t.

$$(\mathbf{a}_{\text{test}} - \mathbf{a}_0) \in \text{span}(\{\mathbf{a}_e - \mathbf{a}_0\}_{e \in [M]}). \quad (4.5)$$

Then the effect of \mathbf{a}_{test} is uniquely identifiable in that

$$\mathbf{X}_{\text{test}} = \mathbf{f}(\mathbf{Z} + W\mathbf{a}_{\text{test}}) \stackrel{d}{=} \widetilde{\mathbf{f}}(\widetilde{\mathbf{Z}} + \widetilde{W}\mathbf{a}_{\text{test}}) \quad (4.6)$$

Remark 4.8 (Additive vs linear perturbations). For our identifiability result it is not necessary that the mean shifts are of the form $W\mathbf{a}_e$. If we replace $W\mathbf{a}_e$ and $\widetilde{W}\mathbf{a}_e$ in (4.1) with arbitrary shift vectors $\mathbf{c}_e, \widetilde{\mathbf{c}}_e \in \mathbb{R}^{d_Z}$, the same result as Thm. 4.1 can be shown to hold with $W\mathbf{A}$ and $\widetilde{W}\mathbf{A}$ replaced by \mathbf{C} and $\widetilde{\mathbf{C}}$, defined as the matrices with columns $(\mathbf{c}_e - \mathbf{c}_0)$ and $(\widetilde{\mathbf{c}}_e - \widetilde{\mathbf{c}}_0)$, respectively. That is, the relative shift vectors are identifiable (up to orthogonal transformation), regardless of whether they are linear in \mathbf{a} . This is relevant, for example, when including nonlinear interactions or learnable element-wise nonlinear dose-response functions $h_j(a_j)$ as in CPA (Lotfollahi et al., 2023). However, linearity is leveraged in the proof of our extrapolation result, where it is used in (4.5) to establish a link between \mathbf{a}_{test} and the training perturbations. Since only \mathbf{a}_{test} is observed at test time, Thm. 4.7 cannot easily be extended to arbitrary shifts, as this would require establishing a link between \mathbf{c}_{test} and the training shifts, all of which are unobserved.

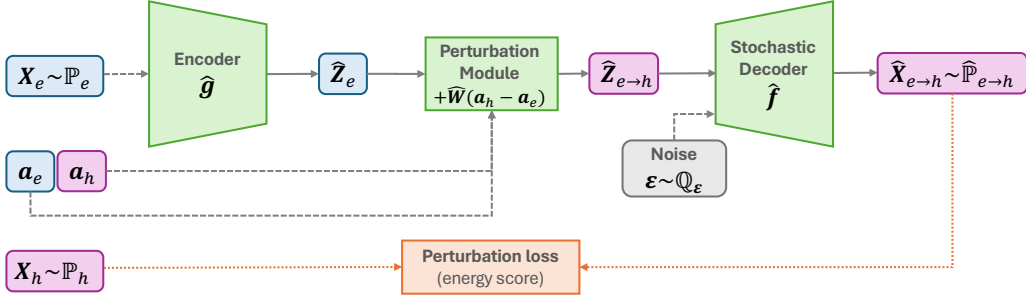


Figure 2. Overview of the perturbation distribution autoencoder (PDAE). A PDAE simulates the distribution of a target perturbation condition h (purple) by encoding, perturbing, and (stochastically) decoding data from a source condition e (blue). Dashed arrows indicate model inputs and green boxes model components with trainable parameters. The learning objective (orange, dotted arrows) amounts to a perturbation loss (bottom), measuring, for all pairs of training domains (e, h) , the dissimilarity between the true distribution of \mathbf{X}_h and its simulated version based on domain e ; At test time, the target perturbation label \mathbf{a}_h can be replaced with an unseen \mathbf{a}_{test} to make predictions.

4.3 Connection to causal representation learning

In causal inference, experimental data resulting from perturbations is modeled via interventions in an underlying causal model. In structural equation models (SEMs; Pearl, 2009; Bongers et al., 2021), interventions modify a subset of assignments that determine each variable from its direct causes and unexplained noise. In general, our model for the effect of perturbations in latent space (§ 3) differs from how interventions are treated in SEMs. However, as summarized in the following result, the class of shift interventions in linear SEMs constitutes a special case of our model class.

Proposition 4.9 (Modeling shift interventions in SEMs). *Consider a linear SEM, $\mathbf{Z} := \mathbf{B}^\top \mathbf{Z} + \boldsymbol{\eta}$, with noise $\boldsymbol{\eta} \sim \mathbb{P}_{\boldsymbol{\eta}}$ and $\mathbf{B} \in \mathbb{R}^{d_Z \times d_Z}$ a weighted adjacency matrix with spectral radius (largest absolute eigenvalue) $\rho(\mathbf{B}) < 1$. Then, the distribution induced by shift interventions $\mathbf{a}_e \in \mathbb{R}^{d_Z}$,*

$$\mathbf{Z} := \mathbf{B}^\top \mathbf{Z} + \boldsymbol{\eta} + \mathbf{a}_e, \quad (4.7)$$

is identical to that induced by (3.1) with $\mathbf{W} = (\mathbf{I} - \mathbf{B}^\top)^{-1}$ and basal state distribution $\mathbb{P}_{\mathbf{Z}} = (\mathbf{I} - \mathbf{B}^\top)^{-1} \mathbb{P}_{\boldsymbol{\eta}}$.

Remark 4.10 (Applicability to cyclic or confounded SEMs). Prop. 4.9 does not require the acyclicity or unconfoundedness (i.e., independence of the noise components) of the SEM. The spectral radius condition (which holds for acyclic systems but is strictly weaker) ensures stability and invertibility of $\mathbf{I} - \mathbf{B}^\top$ (Zheng et al., 2018; Brown et al., 2025).

Combined with a decoder from (3.2), Prop. 4.9 highlights in which sense our model can be interpreted as interventional causal representation learning (Schölkopf et al., 2021; von Kügelgen et al., 2023; Varici et al., 2025) with a linear latent causal model (Squires et al., 2023; Buchholz et al., 2024) and generalized shift interventions (Zhang et al., 2024). For $K = d_Z$ elementary perturbations, the adjacency matrix corresponding to an inferred $\widehat{\mathbf{W}}$ is given by $\widehat{\mathbf{B}} = (\mathbf{I} - \widehat{\mathbf{W}}^{-1})^\top$. However, due to the rotation ambiguity, additional assumptions such as sparse (e.g., single node) shifts would be needed to recover the causal graph induced by the true \mathbf{B} .

5 Perturbation distribution autoencoder

To leverage the extrapolation guarantees of Thm. 4.7, we seek to estimate the identifiable parts of the generative process by matching the distributions of the observed data in (2.1) across all perturbation conditions, as prescribed by condition (4.1) in Thm. 4.1. To this end, we take inspiration from prior distributional learning approaches (Bouchacourt et al., 2016; Shen & Meinshausen, 2024a) and adapt them for multi-domain perturbation modeling. Our method, the *perturbation distribution autoencoder* (PDAE), comprises an encoder, a perturbation matrix, and a (stochastic) decoder, which are trained to maximise the similarity between pairs of true and simulated perturbation distributions, see Fig. 2 for an overview. Intuitively, instead of specifying a (Gaussian, as per Thm. 4.1) prior on the basal state from which to sample latents as in (3.1), we use encoded observations from a source domain as perturbed latents and transform them to perturbed latents from a target domain using the learnt perturbation matrix and the assumed additivity as in (3.1).

Encoder. The encoder $\widehat{\mathbf{g}} : \mathbb{R}^{d_X} \rightarrow \mathbb{R}^{d_Z}$ maps observations \mathbf{x} to the space of perturbation-relevant latents \mathbf{z} . Ideally, it should invert the stochastic mixing function in (3.2) in the sense of recovering the perturbed latent state $\mathbf{z}_{e,i}^{\text{pert}}$ from observation $\mathbf{x}_{e,i}$.¹ We therefore denote the encoder outputs by

$$\widehat{\mathbf{z}}_{e,i}^{\text{pert}} := \widehat{\mathbf{g}}(\mathbf{x}_{e,i}), \quad (5.1)$$

and refer to them as *estimated perturbed latents*.

Perturbation module. If the encoder recovers the perturbed latents up to orthogonal transformation, the additivity of perturbation effects assumed in (3.1) allows us to map between the latent distributions underlying different perturbation conditions. Specifically, we use a perturbation model parametrised by a perturbation matrix $\widehat{\mathbf{W}} \in \mathbb{R}^{d_Z \times K}$

¹This is a key difference to CPA (Lotfollahi et al., 2023) and SAMS-VAE (Bereket & Karaletsos, 2023), which seek an encoder that maps to the latent basal state, regardless of the domain e .

to create *synthetic perturbed latents* from domain h as:

$$\hat{z}_{e \rightarrow h, i}^{\text{pert}} := \hat{z}_{e, i}^{\text{pert}} + \hat{W}(\mathbf{a}_h - \mathbf{a}_e). \quad (5.2)$$

which can be interpreted as undoing the effect of \mathbf{a}_e (i.e., mapping back to the basal state) and then simulating \mathbf{a}_h .

Decoder. The decoder $\hat{f} : \mathbb{R}^{d_z} \times \mathbb{R}^{d_e} \rightarrow \mathbb{R}^{d_x}$ maps estimated perturbed latents \hat{z}^{pert} and noise $\varepsilon \sim \mathbb{Q}_\varepsilon$ to observations. When evaluated on synthetic perturbed latents from (5.2), we refer to the corresponding (random) outputs

$$\hat{\mathbf{X}}_{e \rightarrow h, i} = \hat{f}(\hat{z}_{e \rightarrow h, i}^{\text{pert}}, \varepsilon) \quad \text{where} \quad \varepsilon \sim \mathbb{Q}_\varepsilon \quad (5.3)$$

as *synthetic observations* from domain h based on domain e .

Simulated perturbation distributions. Given a distribution \mathbb{P}_e and the corresponding perturbation label \mathbf{a}_e , our model facilitates sampling synthetic observations for another perturbation condition with label \mathbf{a}_h via (5.2) and (5.3). We denote the corresponding distribution by $\hat{\mathbb{P}}_{e \rightarrow h}$, formally defined as the distribution of

$$\hat{f}(\hat{g}(\mathbf{X}_e) + \hat{W}(\mathbf{a}_h - \mathbf{a}_e), \varepsilon), \quad (5.4)$$

where both $\mathbf{X}_e \sim \mathbb{P}_e$ and $\varepsilon \sim \mathbb{Q}_\varepsilon$ are random. Intuitively, when simulating \mathbb{P}_h based on \mathbb{P}_e via (5.4), the random variable $\hat{g}(\mathbf{X}_e) - \hat{W}\mathbf{a}_e$ in the first argument of \hat{f} plays the role of a random latent basal state from (3.1).

Population-level learning objective. At the population level (i.e., assuming access to the true distributions \mathbb{P}_e), we propose minimizing a sum of pairwise distribution losses,

$$(\hat{g}^*, \hat{f}^*, \hat{W}^*) \in \arg \min_{\hat{g}, \hat{f}, \hat{W}} \sum_{e, h \in [M]_0} d(\hat{\mathbb{P}}_{e \rightarrow h}, \mathbb{P}_h) \quad (5.5)$$

where $\hat{\mathbb{P}}_{e \rightarrow h}$ depends on $(\mathbb{P}_e, \mathbf{a}_e, \mathbf{a}_h)$ and the model parameters via (5.4); and d measures dissimilarity between distributions. We use the negative expected energy score for d ,

$$d(\hat{\mathbb{P}}_{e \rightarrow h}, \mathbb{P}_h) = -\mathbb{E}_{\mathbf{X}_h \sim \mathbb{P}_h} [\text{ES}_\beta(\hat{\mathbb{P}}_{e \rightarrow h}, \mathbf{X}_h)], \quad (5.6)$$

with ES_β (Gneiting & Raftery, 2007) defined as

$$\text{ES}_\beta(\mathbb{P}, \mathbf{x}) = \frac{1}{2} \mathbb{E}_{\mathbf{X}, \mathbf{X}' \stackrel{\text{i.i.d.}}{\sim} \mathbb{P}} \|\mathbf{X} - \mathbf{X}'\|^\beta - \mathbb{E}_{\mathbf{X} \sim \mathbb{P}} \|\mathbf{X} - \mathbf{x}\|^\beta.$$

For $\beta \in (0, 2)$, ES_β is a strictly proper scoring rule, meaning that the expected energy score $\mathbb{E}_{\mathbf{X}}[\text{ES}_\beta(\mathbb{P}, \mathbf{X})]$ is maximized if and only if $\mathbf{X} \sim \mathbb{P}$, see § C.1 for details on probabilistic forecasting and scoring rules. Combined with its computational simplicity, this property makes the negative expected energy score a popular loss function for distributional regression (Bouchacourt et al., 2016; Shen & Meinshausen, 2024b;a; De Bortoli et al., 2025; Shen et al., 2025). It also directly implies the following corollary.

Corollary 5.1. *The objective in (5.5) is minimized if and only if $\mathbb{P}_h = \hat{\mathbb{P}}_{e \rightarrow h}$ for all $e, h \in [M]_0$.*

Training. Since, in practice, we do not have access to the true distributions, we approximate expectations w.r.t. \mathbb{P}_e and \mathbb{P}_h in (5.6) with Monte Carlo estimates based on mini-batches of (2.1), and use a single draw of ε to approximate expectations w.r.t. \mathbb{Q}_ε . We then optimise (5.5) w.r.t. \hat{W} and the parameters of \hat{g} and \hat{f} using stochastic gradient descent (Robbins & Monro, 1951; Kingma & Ba, 2015).

Prediction. To sample from the predicted distribution for a new perturbation label \mathbf{a}_{test} , we use our model to compute the synthetic perturbed test latents $\hat{z}_{e \rightarrow \text{test}, i}^{\text{pert}}$ for all $e \in [M]_0$ and all $i \in [N_e]$ via (5.2), and then sample synthetic test observations $\hat{\mathbf{X}}_{e \rightarrow \text{test}, i}$ according to (5.3). Our estimate of \mathbb{P}_{test} is a convex combination of the domain-specific marginal perturbation distributions $\hat{\mathbb{P}}_{e \rightarrow \text{test}}$ induced by our model for \mathbf{a}_{test} , i.e., the empirical version of

$$\hat{\mathbb{P}}_{\text{test}} = \sum_{e \in [M]_0} \omega_e \hat{\mathbb{P}}_{e \rightarrow \text{test}}. \quad (5.7)$$

with weights $\omega_e \geq 0$ such that $\sum_e \omega_e = 1$ to account for prior knowledge or differing sample sizes across domains; common approaches include uniform weighting ($\omega_e = \frac{1}{M+1}$) or using only control observations ($\omega_e = 0$ for $e \neq 0$).

Full algorithm and extensions. Due to space constraints, we present only the core PDAE architecture here; for additional loss components which may help in practice but are not used in our simulations (a reconstruction objective, latent prior, and sparsity regularization), a complete algorithm, and a discussion of goodness of fit testing, see § B.

6 Related work

Biological perturbation models. Our model from § 3 is closely related to prior work on modeling combinations of genetic or chemical perturbations. CPA (Lotfollahi et al., 2023) employs an adversarial autoencoder for estimation, see § C.4 for details. SVAE+ (Lopez et al., 2023) and SAMS-VAE (Bereket & Karaletsos, 2023) instead fit a generative model by maximising the evidence lower bound (ELBO; a lower bound to the marginal likelihood) within the variational autoencoder (VAE) framework (Kingma & Welling, 2014; Rezende et al., 2014). This requires evaluating the likelihood $p(\mathbf{x}|\mathbf{z})$, and thus generally comes with parametric assumptions. In contrast, PDAE is based on classical (non-variational) autoencoders and is trained using the energy score, which only requires being able to sample from the stochastic decoder. Both SVAE+ and SAMS-VAE additionally assume that the effects of perturbations on the latents are sparse (cf. § B). SAMS-VAE and CPA adopt the same compositional perturbation model as (3.1), wherein the effect of perturbations can be decomposed into a sum of effects of elementary perturbations, captured by the linear form $\mathbf{W}\mathbf{a}$. In contrast, SVAE+ extends work on identifiable VAEs with sparsely changing mechanisms (Lachapelle et al., 2022; 2024) and models each perturbation condition

Table 1. Results on synthetic 2D data. We report average performances over 7 ID and 14 OOD test cases; shown are the mean \pm one standard deviation over 5 random seeds. Best results are highlighted in bold. Theoretical guarantees for PDAE rely on distributional overlap in the latent space (ID); no method is expected to perform well on OOD test cases.

Method	In-Distribution (ID) Test			Out-of-Distribution (OOD) Test		
	ED (↓)	MMD (↓)	$\ \mu_x - \hat{\mu}^x\ _2$ (↓)	ED (↓)	MMD (↓)	$\ \mu_x - \hat{\mu}^x\ _2$ (↓)
Pool All	$0.855 \pm .005$	$0.557 \pm .004$	$0.441 \pm .001$	$1.908 \pm .004$	$1.266 \pm .004$	$1.298 \pm .002$
Pseudobulking	$0.596 \pm .004$	$0.716 \pm .006$	$0.382 \pm .002$	$1.130 \pm .005$	$0.965 \pm .006$	$0.894 \pm .004$
Linear Regression	$0.069 \pm .001$	$0.181 \pm .003$	$0.131 \pm .003$	$0.536 \pm .010$	$0.808 \pm .012$	$0.524 \pm .007$
CPA	$0.600 \pm .239$	$1.152 \pm .287$	$0.516 \pm .165$	$1.538 \pm .261$	$1.885 \pm .241$	$1.132 \pm .171$
PDAE (Ours)	$0.001 \pm .000$	$0.003 \pm .001$	$0.012 \pm .003$	$0.018 \pm .006$	$0.029 \pm .007$	$0.090 \pm .017$

separately. None of these prior perturbation models provide theoretical identifiability or extrapolation guarantees.

Testing for and modeling interactions. Xu et al. (2024) propose tests for the hypothesis of no (nonlinear) interactions in latent space, based on the assumption that perturbations affect disjoint latents and given suitable data from both individual and pairs of perturbations. Adduri et al. (2025) and He et al. (2025) propose modeling interactions via attention in transformer-based architectures (Vaswani et al., 2017).

Causal approaches. Zhang et al. (2024) and Liu et al. (2025) consider perturbation extrapolation from a causal representation learning perspective. They model elementary perturbations as shift interventions and use a VAE-based approach, which, similar to PDAE, is trained primarily to maximise the similarity between real and simulated perturbation distributions. Schneider et al. (2025) instead model interventions directly at the level of measurements.

Identifiable representation learning for extrapolation. Saengkyongam et al. (2024, §4) consider an identifiability problem similar to the one we study in § 4 and leverage affine identifiability to derive out-of-support extrapolation guarantees. However, their model and proof strategy differ from ours, e.g., by requiring the training support of perturbations \mathbf{a} to contain a non-empty open subset of \mathbb{R}^K .

7 Simulation study

In this section, we investigate the empirical performance of PDAE through a controlled simulation with synthetic data.

Methods. We compare our approach with CPA (Lotfollahi et al., 2023) and the following baselines:

- *Pool all*: output the distribution and mean obtained by pooling all training observations;
- *Pseudobulking*: like *Pool All* but pool only training data arising from individual perturbations involved in the combination to be predicted (e.g., pool data from $(1, 0, 0)^\top$ and $(0, 1, 0)^\top$ to predict $\mathbf{a}_{\text{test}} = (1, 1, 0)^\top$);
- *Linear regression*: linearly regress the domain-specific means of observations $\mu_e^x \in \mathbb{R}^{d_x}$ on \mathbf{a}_e and use the resulting model to predict the test mean μ_{test}^x from \mathbf{a}_{test} .

The former two were also used by Lotfollahi et al. (2023); we propose the latter as an additional (stronger) baseline. Since CPA and linear regression only predict a mean, in these cases, we apply the test mean shift to all observations in the reference condition to simulate the test distribution and use this to compute distributional similarity metrics.

Metrics. To assess the distributional fit between predicted and true (empirical) test distributions, we use the energy distance (ED; Székely & Rizzo, 2013), i.e., twice the normalized negative expected (marginal) energy score, and the maximum mean discrepancy (MMD; Gretton et al., 2012) with Gaussian kernel and bandwidth chosen by the median heuristic, see § C.2 for more on measures of distributional similarity. Since some methods are primarily designed for mean prediction, we also report the L2 norm of the difference between the predicted and true mean, $\|\mu^x - \hat{\mu}^x\|$.

Data. For ease of visualization, we first consider the case of $d_Z = d_X = 2$ -dimensional latents and observations. The base distribution \mathbb{P}_Z is a zero-mean, isotropic Gaussian with standard deviation $\sigma = 0.25$. We consider $K = 3$ elementary perturbations with associated shift vectors $\mathbf{w}_1 = (1, 0)^\top$, $\mathbf{w}_2 = (0, 1)^\top$, and $\mathbf{w}_3 = (1, 1)^\top$ and create $M + 1 = 4$ training domains with perturbation labels $\mathbf{a}_0 = (0, 0, 0)^\top$, $\mathbf{a}_1 = (1, 0, 0)^\top$, $\mathbf{a}_2 = (0, 1, 0)^\top$, and $\mathbf{a}_3 = (0, 0, 1)^\top$. In this case, the sufficient diversity condition (iii) used to establish identifiability in Thm. 4.1 is satisfied. For testing, we distinguish two scenarios: in-distribution (ID) and out-of-distribution (OOD) test cases, depending on whether the perturbed latents resulting from \mathbf{a}_{test} lie mostly within or outside the support of the empirical distributions of perturbed training latents, respectively. We consider 14 randomly generated ID and OOD test cases each, see Fig. 9 and § D for a visualization and further details. To generate observations, we use the complex exponential $\mathbf{x} = \mathbf{f}(\mathbf{z}) = e^{z_1}(\cos z_2, \sin z_2)$ as a deterministic nonlinear mixing function.

Experimental details. We generate $N_e = 2^{14}$ observations for each domain. Both CPA and PDAE use 4-hidden-layer MLPs with 64 hidden units as encoders and decoders, a $\widehat{d}_Z = 2$ -dimensional latent space, and are trained for 2000 epochs using a batch size of 2^{12} . For PDAE, we set the energy score exponent $\beta = 1$ and use a learning rate of 0.005.

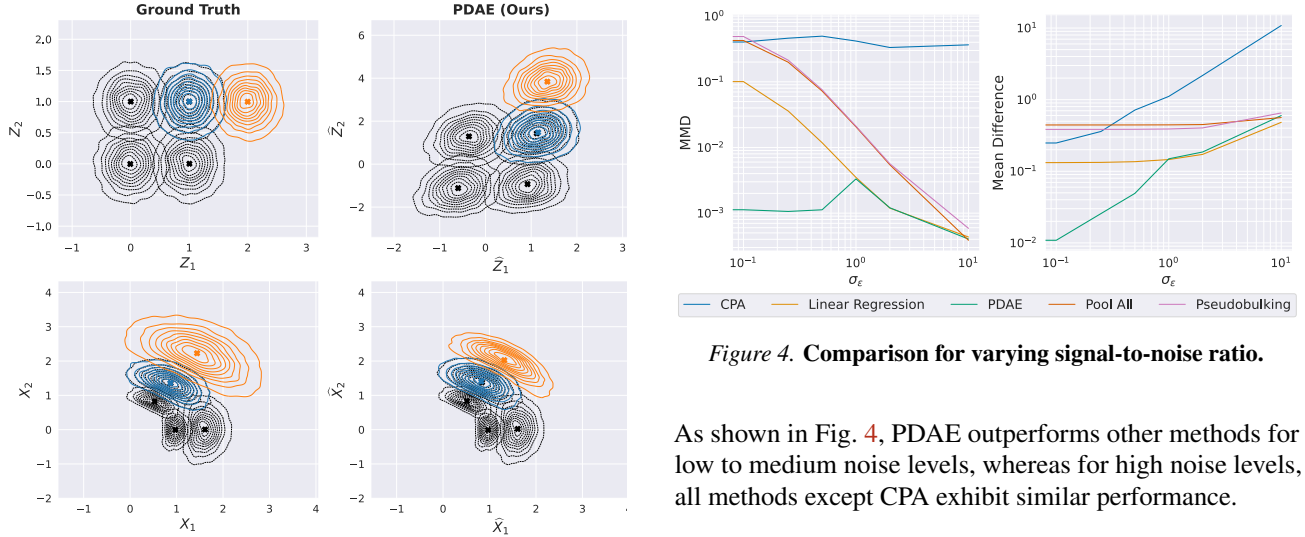


Figure 3. Qualitative results. Shown are kernel density estimates of the training data (black); an ID test case (blue) with $\alpha_{\text{test}}^{\text{ID}} = (1, 1, 0)^\top$, which was not seen during training but induces the same perturbed latent distribution as α_3 ; and an OOD test case (orange) with $\alpha_{\text{test}}^{\text{OOD}} = (1, 0, 1)^\top$. PDAE recovers an affine transformation—since condition (ii) of Thm. 4.1 is not enforced, cf. § A.1—of the true latents (top row) leading to accurate distributional predictions for the training and ID test domains (bottom row). In the OOD case, the test distribution in latent space is identified but supported in a space that was mostly not seen during training (orange, top right). As a result, the corresponding decoder output does not accurately match the true OOD distribution (orange, bottom row).

For CPA, we choose a 1-hidden-layer MLP with 64 hidden units for the adversarial classifier. For the remaining hyperparameters, we randomly sample 100 joint configurations and choose the one with the smallest MMD across 7 ID test cases, see § D for details. We report results for average performance across the remaining 7 ID and 14 OOD test cases over 5 repetitions of randomly generating data and initializing, training, and evaluating models.

Results. The results are shown in Tab. 1. For the ID test setting, PDAE performs best, achieving a near-perfect distributional fit. CPA outperforms the pooling and pseudobulking baselines (consistent with results reported by Lotfollahi et al. (2023) on gene perturbation data), but does substantially worse than linear regression and PDAE at both mean and distributional prediction. For the OOD test setting, all methods expectedly perform worse, with PDAE yielding the least bad performance,² see Fig. 3 and its caption for details.

Noisy observations. We additionally consider a modified version of the aforementioned experiment with $d_X = 10$ (instead of $d_X = 2$) observed dimensions by concatenating $d_\epsilon = 8$ additional dimensions of mean-zero Gaussian noise and investigate the behavior for increasing noise variance (i.e., decreasing signal-to-noise ratio), see § D.2 for details.

²We believe that PDAE benefits from implicit regularization in the network and that worse counterexamples can be constructed.

As shown in Fig. 4, PDAE outperforms other methods for low to medium noise levels, whereas for high noise levels, all methods except CPA exhibit similar performance.

8 Discussion, limitations, and future work

Necessity of Gaussianity. Gaussianity of \mathbb{P}_Z is sufficient to prove identifiability, but may not be necessary. Indeed, PDAE does not explicitly enforce any particular latent distribution, but still yields good performance. To impose a specific prior such as that from assumption (ii) of Thm. 4.1, one can penalize deviations of the encoded basal state distributions from the prior, e.g., using the energy score as discussed in § B. Based on preliminary results with Laplacian basal states, we hypothesize that our results can be generalized to other distributions from the exponential family.

Decoder extrapolation. The need for the decoder to generalize to new inputs poses a challenge for distributional perturbation extrapolation. While this issue is absent from our theory, where \mathbb{P}_Z is Gaussian and thus has full support, it arises in practice when learning from finite data. As discussed in Fig. 3, this issue is orthogonal to learning the correct representation and perturbation model. However, it should be possible to realize that the distribution of perturbed test latents lies (partially) outside the training support. Thus, quantifying the uncertainty associated with different parts of the predicted distribution in observation space may become possible, e.g., by measuring the overlap in supports or relying on outlier and anomaly detection methods.

Modeling gene expression. Our results from Fig. 4 that methods become indistinguishable for low signal-to-noise ratio are consistent with similar findings in the context of noisy high-dimensional gene perturbation data (Ahmann-Eltze et al., 2025; Viñas Torné et al., 2025), highlighting the need for better calibrated and interpretable evaluation metrics (Miller et al., 2025; Mejia et al., 2025). Future work should seek to more explicitly incorporate cell-type variation, the zero-inflated nature of gene expression data, and the limited effectiveness of CRISPR perturbations (Hugi et al., 2025) into PDAE and advance our theoretical understanding of extrapolation in the presence of nonlinear interactions.

Impact Statement

This paper presents work whose goal is to advance the field of Machine Learning. There are many potential societal consequences of our work, none which we feel must be specifically highlighted here.

References

Adduri, A. K., Gautam, D., Bevilacqua, B., Imran, A., Shah, R., Naghipourfar, M., Teyssier, N., Ilango, R., Nagaraj, S., Dong, M., et al. Predicting cellular responses to perturbation across diverse contexts with state. *BioRxiv*, pp. 2025–06, 2025. [Cited on p. 1 and 7.]

Ahlmann-Eltze, C., Huber, W., and Anders, S. Deep-learning-based gene perturbation effect prediction does not yet outperform simple linear baselines. *Nature Methods*, pp. 1–5, 2025. [Cited on p. 8.]

Baringhaus, L. and Franz, C. On a new multivariate two-sample test. *Journal of Multivariate Analysis*, 88(1): 190–206, 2004. [Cited on p. 20.]

Belkin, M. and Niyogi, P. Laplacian eigenmaps and spectral techniques for embedding and clustering. In *Advances in Neural Information Processing Systems*, volume 14, 2001. [Cited on p. 21.]

Bengio, Y., Courville, A., and Vincent, P. Representation learning: A review and new perspectives. *IEEE Transactions on Pattern Analysis and Machine Intelligence*, 35(8):1798–1828, 2013. [Cited on p. 21.]

Bereket, M. and Karaletsos, T. Modelling cellular perturbations with the sparse additive mechanism shift variational autoencoder. In *Advances in Neural Information Processing Systems*, volume 36, pp. 1–12, 2023. [Cited on p. 1, 3, 5, 6, and 18.]

Bongers, S., Forre, P., Peters, J., and Mooij, J. M. Foundations of structural causal models with cycles and latent variables. *Annals of Statistics*, 49(5):2885–2915, 2021. [Cited on p. 5.]

Bouchacourt, D., Mudigonda, P. K., and Nowozin, S. Disco nets: Dissimilarity coefficients networks. In *Advances in Neural Information Processing Systems*, volume 29, 2016. [Cited on p. 5 and 6.]

Brady, J., Zimmermann, R. S., Sharma, Y., Schölkopf, B., von Kügelgen, J., and Brendel, W. Provably learning object-centric representations. In *International Conference on Machine Learning*, pp. 3038–3062. PMLR, 2023. [Cited on p. 3.]

Brady, J., von Kügelgen, J., Lachapelle, S., Buchholz, S., Kipf, T., and Brendel, W. Interaction asymmetry: A general principle for learning composable abstractions. In *International Conference on Learning Representations*, 2025. [Cited on p. 3.]

Brown, B. C., Tokolyi, A., Morris, J. A., Lappalainen, T., and Knowles, D. A. Large-scale causal discovery using interventional data sheds light on gene network structure in k562 cells. *Nature Communications*, 16(1):9628, 2025. [Cited on p. 5.]

Buchholz, S., Rajendran, G., Rosenfeld, E., Aragam, B., Schölkopf, B., and Ravikumar, P. Learning linear causal representations from interventions under general nonlinear mixing. In *Advances in Neural Information Processing Systems*, volume 36, 2024. [Cited on p. 5.]

Bunne, C., Stark, S. G., Gut, G., Del Castillo, J. S., Levesque, M., Lehmann, K.-V., Pelkmans, L., Krause, A., and Rätsch, G. Learning single-cell perturbation responses using neural optimal transport. *Nature methods*, 20(11), 2023. [Cited on p. 1.]

Cayton, L. Algorithms for manifold learning, 2005. Technical Report, University of California at San Diego. [Cited on p. 21.]

De Bortoli, V., Galashov, A., Guntupalli, J. S., Zhou, G., Murphy, K., Gretton, A., and Doucet, A. Distributional diffusion models with scoring rules. In *International Conference on Machine Learning*, 2025. [Cited on p. 6.]

Dixit, A., Parnas, O., Li, B., Chen, J., Fulco, C. P., Jerby-Arnon, L., Marjanovic, N. D., et al. Perturb-seq: dissecting molecular circuits with scalable single-cell RNA profiling of pooled genetic screens. *cell*, 167(7):1853–1866, 2016. [Cited on p. 1.]

Dong, K. and Ma, T. First steps toward understanding the extrapolation of nonlinear models to unseen domains. In *International Conference on Learning Representations*, 2022. [Cited on p. 3.]

Gneiting, T. and Raftery, A. E. Strictly proper scoring rules, prediction, and estimation. *Journal of the American Statistical Association*, 102(477):359–378, 2007. [Cited on p. 2, 3, 6, and 20.]

Goyal, A. and Bengio, Y. Inductive biases for deep learning of higher-level cognition. *Proceedings of the Royal Society A*, 478(2266):20210068, 2022. [Cited on p. 3.]

Gretton, A., Borgwardt, K. M., Rasch, M. J., Schölkopf, B., and Smola, A. A kernel two-sample test. *The Journal of Machine Learning Research*, 13(1):723–773, 2012. [Cited on p. 7 and 20.]

He, C., Zhang, J., Dahleh, M., and Uhler, C. Morph predicts the single-cell outcome of genetic perturbations across

conditions and data modalities. *bioRxiv*, 2025. [Cited on p. 1 and 7.]

Hetzel, L., Boehm, S., Kilbertus, N., Günemann, S., and Theis, F. Predicting cellular responses to novel drug perturbations at a single-cell resolution. In *Advances in Neural Information Processing Systems*, volume 35, pp. 26711–26722, 2022. [Cited on p. 1.]

Hinton, G. E. and Salakhutdinov, R. R. Reducing the dimensionality of data with neural networks. *science*, 313 (5786):504–507, 2006. [Cited on p. 21.]

Hugi, F., Tanna, T., Platt, R. J., and Rätsch, G. Perturbation-aware representation learning for in vivo genetic screens. *bioRxiv*, pp. 2025–10, 2025. [Cited on p. 1 and 8.]

Jinek, M., Chylinski, K., Fonfara, I., Hauer, M., Doudna, J. A., and Charpentier, E. A programmable dual-RNA–guided DNA endonuclease in adaptive bacterial immunity. *science*, 337(6096):816–821, 2012. [Cited on p. 1.]

Kamimoto, K., Stringa, B., Hoffmann, C. M., Jindal, K., Solnica-Krezel, L., and Morris, S. A. Dissecting cell identity via network inference and in silico gene perturbation. *Nature*, 614(7949):742–751, 2023. [Cited on p. 1.]

Khemakhem, I., Kingma, D., Monti, R., and Hyvarinen, A. Variational autoencoders and nonlinear ica: A unifying framework. In *International Conference on Artificial Intelligence and Statistics*, pp. 2207–2217, 2020. [Cited on p. 4.]

Kingma, D. P. and Ba, J. Adam: A method for stochastic optimization. In *International Conference on Learning Representations*, 2015. [Cited on p. 6.]

Kingma, D. P. and Welling, M. Auto-encoding variational Bayes. In *International Conference on Learning Representations*, 2014. [Cited on p. 6.]

Koenker, R. and Bassett Jr, G. Regression quantiles. *Econometrica: Journal of the Econometric Society*, pp. 33–50, 1978. [Cited on p. 3.]

Lachapelle, S., Rodriguez, P., Sharma, Y., Everett, K. E., Le Priol, R., Lacoste, A., and Lacoste-Julien, S. Disentanglement via mechanism sparsity regularization: A new principle for nonlinear ica. In *Conference on Causal Learning and Reasoning*, pp. 428–484. PMLR, 2022. [Cited on p. 6.]

Lachapelle, S., Mahajan, D., Mitliagkas, I., and Lacoste-Julien, S. Additive decoders for latent variables identification and cartesian-product extrapolation. In *Advances in Neural Information Processing Systems*, volume 36, 2023. [Cited on p. 3.]

Lachapelle, S., López, P. R., Sharma, Y., Everett, K., Priol, R. L., Lacoste, A., and Lacoste-Julien, S. Nonparametric partial disentanglement via mechanism sparsity: Sparse actions, interventions and sparse temporal dependencies. *arXiv preprint arXiv:2401.04890*, 2024. [Cited on p. 6.]

Lake, B. M., Ullman, T. D., Tenenbaum, J. B., and Gershman, S. J. Building machines that learn and think like people. *Behavioral and brain sciences*, 40:e253, 2017. [Cited on p. 3.]

Lample, G., Zeghidour, N., Usunier, N., Bordes, A., Denoyer, L., and Ranzato, M. Fader networks: Manipulating images by sliding attributes. In *Advances in Neural Information Processing Systems*, volume 30, 2017. [Cited on p. 22.]

Lippl, S. and Stachenfeld, K. When does compositional structure yield compositional generalization? a kernel theory. *arXiv preprint arXiv:2405.16391*, 2024. [Cited on p. 3.]

Liu, E., Zhang, J., and Uhler, C. Learning genetic perturbation effects with variational causal inference. *bioRxiv*, pp. 2025–06, 2025. [Cited on p. 7.]

Lopez, R., Regier, J., Cole, M. B., Jordan, M. I., and Yosef, N. Deep generative modeling for single-cell transcriptomics. *Nature methods*, 15(12):1053–1058, 2018. [Cited on p. 1 and 3.]

Lopez, R., Tagasovska, N., Ra, S., Cho, K., Pritchard, J., and Regev, A. Learning causal representations of single cells via sparse mechanism shift modeling. In *Conference on Causal Learning and Reasoning*, pp. 662–691. PMLR, 2023. [Cited on p. 1, 3, and 6.]

Lotfollahi, M., Wolf, F. A., and Theis, F. J. scgen predicts single-cell perturbation responses. *Nature methods*, 16 (8):715–721, 2019. [Cited on p. 1.]

Lotfollahi, M., Klimovskaia Susmelj, A., De Donno, C., Hetzel, L., Ji, Y., Ibarra, I. L., Srivatsan, S. R., Naghipourfar, M., Daza, R. M., Martin, B., Shendure, J., McFaline-Figueroa, J. L., Boyeau, P., Wolf, F. A., Yakubova, N., Günemann, S., Trapnell, C., Lopez-Paz, D., and Theis, F. J. Predicting cellular responses to complex perturbations in high-throughput screens. *Molecular Systems Biology*, 19(6):e11517, 2023. [Cited on p. 1, 3, 4, 5, 6, 7, 8, 22, and 23.]

Matheson, J. E. and Winkler, R. L. Scoring rules for continuous probability distributions. *Management Science*, 22 (10):1087–1096, 1976. [Cited on p. 20.]

Mejia, G. M., Miller, H. E., Leblanc, F. J., Wang, B., Swain, B., and Camillo, L. P. d. L. Diversity by design: Addressing mode collapse improves scRNA-seq perturbation

modeling on well-calibrated metrics. *arXiv preprint arXiv:2506.22641*, 2025. [Cited on p. 8.]

Miller, H. E., Mejia, G. M., Leblanc, F. J., Wang, B., Swain, B., and Camillo, L. P. d. L. Deep learning-based genetic perturbation models do outperform uninformative baselines on well-calibrated metrics. *bioRxiv*, pp. 2025–10, 2025. [Cited on p. 8.]

Montero, M. L., Ludwig, C. J., Costa, R. P., Malhotra, G., and Bowers, J. The role of disentanglement in generalisation. In *International Conference on Learning Representations*, 2021. [Cited on p. 3.]

Montero, M. L., Bowers, J., Costa, R. P., Ludwig, C. J., and Malhotra, G. Lost in latent space: Examining failures of disentangled models at combinatorial generalisation. In Oh, A. H., Agarwal, A., Belgrave, D., and Cho, K. (eds.), *Advances in Neural Information Processing Systems*, 2022. [Cited on p. 3.]

Norman, T. M., Horlbeck, M. A., Replogle, J. M., Ge, A. Y., Xu, A., Jost, M., Gilbert, L. A., and Weissman, J. S. Exploring genetic interaction manifolds constructed from rich single-cell phenotypes. *science*, 365(6455):786–793, 2019. [Cited on p. 1.]

Pearl, J. *Causality: Models, Reasoning, and Inference*. Cambridge University Press, 2nd edition, 2009. [Cited on p. 5.]

Peters, J., Janzing, D., and Schölkopf, B. *Elements of Causal Inference: Foundations and Learning Algorithms*. MIT Press, 2017. [Cited on p. 3.]

Qi, X., Zhao, L., Tian, C., Li, Y., Chen, Z.-L., Huo, P., Chen, R., Liu, X., Wan, B., Yang, S., et al. Predicting transcriptional responses to novel chemical perturbations using deep generative model for drug discovery. *Nature Communications*, 15(1):1–19, 2024. [Cited on p. 1.]

Rezende, D. J., Mohamed, S., and Wierstra, D. Stochastic backpropagation and approximate inference in deep generative models. In *International Conference on Machine Learning*, pp. 1278–1286, 2014. [Cited on p. 6.]

Robbins, H. and Monro, S. A stochastic approximation method. *The Annals of Mathematical Statistics*, pp. 400–407, 1951. [Cited on p. 6.]

Roohani, Y., Huang, K., and Leskovec, J. Predicting transcriptional outcomes of novel multigene perturbations with gears. *Nature Biotechnology*, 42(6):927–935, 2024. [Cited on p. 1.]

Rumelhart, D. E., Hinton, G. E., and Williams, R. J. Learning representations by back-propagating errors. *nature*, 323(6088):533–536, 1986. [Cited on p. 21.]

Saengkyongam, S., Rosenfeld, E., Ravikumar, P. K., Pfister, N., and Peters, J. Identifying representations for intervention extrapolation. In *International Conference on Learning Representations*, 2024. [Cited on p. 7.]

Saul, L. K. and Roweis, S. T. Think globally, fit locally: Unsupervised learning of low dimensional manifolds. *Journal of Machine Learning Research*, 4:119–155, 2003. [Cited on p. 21.]

Schneider, N., Lorch, L., Kilbertus, N., Schölkopf, B., and Krause, A. Generative intervention models for causal perturbation modeling. In *International Conference on Machine Learning*, 2025. [Cited on p. 7.]

Schölkopf, B. and Smola, A. J. *Learning with kernels: support vector machines, regularization, optimization, and beyond*. MIT press, 2002. [Cited on p. 20.]

Schölkopf, B., Locatello, F., Bauer, S., Ke, N. R., Kalchbrenner, N., Goyal, A., and Bengio, Y. Toward causal representation learning. *Proceedings of the IEEE*, 109(5):612–634, 2021. [Cited on p. 5.]

Schott, L., von Kügelgen, J., Träuble, F., Gehler, P. V., Russell, C., Bethge, M., Schölkopf, B., Locatello, F., and Brendel, W. Visual representation learning does not generalize strongly within the same domain. In *International Conference on Learning Representations*, 2022. [Cited on p. 3.]

Sejdinovic, D., Sriperumbudur, B., Gretton, A., and Fukumizu, K. Equivalence of distance-based and rkhs-based statistics in hypothesis testing. *The Annals of Statistics*, pp. 2263–2291, 2013. [Cited on p. 21.]

Shen, X. and Meinshausen, N. Distributional principal autoencoders. *arXiv preprint arXiv:2404.13649*, 2024a. [Cited on p. 5, 6, 18, 19, and 21.]

Shen, X. and Meinshausen, N. Egression: extrapolation through the lens of distributional regression. *Journal of the Royal Statistical Society Series B: Statistical Methodology*, 2024b. [Cited on p. 6.]

Shen, X., Meinshausen, N., and Zhang, T. Reverse markov learning: Multi-step generative models for complex distributions. *arXiv preprint arXiv:2502.13747*, 2025. [Cited on p. 6.]

Sohn, K., Lee, H., and Yan, X. Learning structured output representation using deep conditional generative models. In *Advances in Neural Information Processing Systems*, volume 28, 2015. [Cited on p. 3.]

Squires, C., Seigal, A., Bhat, S., and Uhler, C. Linear causal disentanglement via interventions. In *40th International Conference on Machine Learning*, 2023. [Cited on p. 5.]

Székely, G. J. and Rizzo, M. L. Energy statistics: A class of statistics based on distances. *Journal of Statistical Planning and Inference*, 143(8):1249–1272, 2013. [Cited on p. 7 and 20.]

Tenenbaum, J. B., Silva, V. d., and Langford, J. C. A global geometric framework for nonlinear dimensionality reduction. *science*, 290(5500):2319–2323, 2000. [Cited on p. 21.]

Varici, B., Acartürk, E., Shanmugam, K., Kumar, A., and Tajer, A. Score-based causal representation learning: Linear and general transformations. *Journal of Machine Learning Research*, 26(112):1–90, 2025. [Cited on p. 5.]

Vaswani, A., Shazeer, N., Parmar, N., Uszkoreit, J., Jones, L., Gomez, A. N., Kaiser, Ł., and Polosukhin, I. Attention is all you need. In *Advances in Neural Information Processing Systems*, volume 30, 2017. [Cited on p. 7.]

Viñas Torné, R., Wiatrak, M., Piran, Z., Fan, S., Jiang, L., Teichmann, S. A., Nitzan, M., and Brbić, M. Systema: a framework for evaluating genetic perturbation response prediction beyond systematic variation. *Nature Biotechnology*, pp. 1–10, 2025. [Cited on p. 8.]

von Kügelen, J., Besserve, M., Wendong, L., Gresele, L., Kekić, A., Bareinboim, E., Blei, D., and Schölkopf, B. Nonparametric identifiability of causal representations from unknown interventions. In *Advances in Neural Information Processing Systems*, volume 36, pp. 48603–48638, 2023. [Cited on p. 5.]

Wang, Z., Gerstein, M., and Snyder, M. RNA-seq: a revolutionary tool for transcriptomics. *Nature reviews genetics*, 10(1):57–63, 2009. [Cited on p. 1.]

Wiedemer, T., Brady, J., Panfilov, A., Juhos, A., Bethge, M., and Brendel, W. Provable compositional generalization for object-centric learning. In *International Conference on Learning Representations*, 2024a. [Cited on p. 3.]

Wiedemer, T., Mayilvahanan, P., Bethge, M., and Brendel, W. Compositional generalization from first principles. In *Advances in Neural Information Processing Systems*, volume 36, 2024b. [Cited on p. 3.]

Xu, Z., Jain, M., Denton, A., Whitfield, S., Didolkar, A., Earnshaw, B., and Hartford, J. S. Automated discovery of pairwise interactions from unstructured data. *arXiv preprint arXiv:2409.07594*, 2024. [Cited on p. 7.]

Yu, H. and Welch, J. D. Perturbnet predicts single-cell responses to unseen chemical and genetic perturbations. *BioRxiv*, pp. 2022–07, 2022. [Cited on p. 1.]

Zhang, J., Greenwald, K., Squires, C., Srivastava, A., Shanmugam, K., and Uhler, C. Identifiability guarantees for causal disentanglement from soft interventions. *Advances in Neural Information Processing Systems*, 36, 2024. [Cited on p. 5 and 7.]

Zhang, J., Ubas, A. A., de Borja, R., Svensson, V., Thomas, N., Thakar, N., Lai, I., Winters, A., Khan, U., Jones, M. G., et al. Tahoe-100m: A giga-scale single-cell perturbation atlas for context-dependent gene function and cellular modeling. *BioRxiv*, pp. 2025–02, 2025. [Cited on p. 1.]

Zheng, X., Aragam, B., Ravikumar, P. K., and Xing, E. P. Dags with no tears: Continuous optimization for structure learning. In *Advances in Neural Information Processing Systems*, volume 31, 2018. [Cited on p. 5.]

Appendices

Table of Contents

A Proofs	13
A.1 Proof of reparametrizability without loss of generality	13
A.2 Proof of Thm. 4.1	14
A.3 Proof of Cor. 4.2	16
A.4 Proof of Thm. 4.7	16
A.5 Proof of Prop. 4.9	17
B PDAE training: Additional losses and complete algorithm	17
C Additional background material and related work	20
C.1 Probabilistic forecasting and scoring rules	20
C.2 Assessing distributional similarity	20
C.3 Representation learning	21
C.4 Perturbation modeling	22
D Additional experimental details and results	23
D.1 Hyperparameter selection for CPA	23
D.2 Robustness experiment with varying signal-to-noise ratio	23
D.3 Details on validation and test cases	25

A Proofs

A.1 Proof of reparametrizability without loss of generality

We first state and prove the following lemma, which shows that the choices of means and covariances of the base distribution in assumption (ii) of Thm. 4.1 come without loss of generality (w.l.o.g.).

Lemma A.1. *Let f and W be such that assumptions (i)–(iii) of Thm. 4.1 are satisfied, and let $\mathbb{P} = \mathcal{N}(\mu, \Sigma)$ with positive definite covariance matrix Σ . Then there exist \tilde{f} and \tilde{W} such that \tilde{f} , \tilde{W} , and $\tilde{\mathbb{P}} = \mathcal{N}(-\tilde{W}a_0, I)$ generates the same distributions, i.e.,*

$$\forall e \in [M]_0 : \quad f(Z + Wa_e) \stackrel{d}{=} \tilde{f}(\tilde{Z} + \tilde{W}a_e), \quad \text{where } Z \sim \mathcal{N}(\mu, \Sigma) \text{ and } \tilde{Z} \sim \mathcal{N}(-\tilde{W}a_0, I), \quad (\text{A.1})$$

with \tilde{f} and \tilde{W} also satisfying assumptions (i) and (iii) of Thm. 4.1.

Proof. Define $\tilde{f} : z \mapsto f(\mu + Wa_0 + \Sigma^{\frac{1}{2}}z)$ and let $\tilde{W} := \Sigma^{-\frac{1}{2}}W$. The equality in distribution in (A.1) then follows directly by substitution from the properties of linear transformations of Gaussians. Since f is a C^2 diffeomorphism by assumption, so is \tilde{f} , since it is the composition of f with an affine function. Moreover, since Σ (and thus also any inverse square root $\Sigma^{-\frac{1}{2}}$) is invertible, we have $\text{rank}(\tilde{W}A) = \text{rank}(WA)$ and thus assumption (iii) also holds. \square

A.2 Proof of Thm. 4.1

Theorem 4.1 (Identifiability up to orthogonal transformation). *For $M \in \mathbb{Z}_{\geq 0}$, let $\mathbf{a}_0, \dots, \mathbf{a}_M \in \mathbb{R}^K$ be $M + 1$ perturbation labels. Let $\mathbf{f}, \tilde{\mathbf{f}} : \mathbb{R}^{d_Z} \rightarrow \mathbb{R}^{d_X}$, $\mathbf{W}, \tilde{\mathbf{W}} \in \mathbb{R}^{d_Z \times K}$, and $\mathbb{P}, \tilde{\mathbb{P}}$ be distributions on \mathbb{R}^{d_Z} such that the models $(\mathbf{f}, \mathbf{W}, \mathbb{P})$ and $(\tilde{\mathbf{f}}, \tilde{\mathbf{W}}, \tilde{\mathbb{P}})$ induce the same observed distributions, i.e., for all $e \in [M]_0$:*

$$\mathbf{f}(\mathbf{Z} + \mathbf{W}\mathbf{a}_e) \stackrel{d}{=} \tilde{\mathbf{f}}(\tilde{\mathbf{Z}} + \tilde{\mathbf{W}}\mathbf{a}_e), \quad (4.1)$$

with $\mathbf{Z} \sim \mathbb{P}$ and $\tilde{\mathbf{Z}} \sim \tilde{\mathbb{P}}$ independent. Assume further that:

- (i) **[invertibility]** \mathbf{f} and $\tilde{\mathbf{f}}$ are C^2 -diffeomorphisms onto their respective images;
- (ii) **[Gaussianity]** \mathbf{Z} and $\tilde{\mathbf{Z}}$ are standard isotropic multivariate Gaussians with means chosen such that the latent distributions in domain $e = 0$ are centered at the origin, i.e., $\mathbb{P} = \mathcal{N}(-\mathbf{W}\mathbf{a}_0, \mathbf{I})$ and $\tilde{\mathbb{P}} = \mathcal{N}(-\tilde{\mathbf{W}}\mathbf{a}_0, \mathbf{I})$;
- (iii) **[sufficient diversity]** the matrix $\tilde{\mathbf{W}}\mathbf{A} \in \mathbb{R}^{d_Z \times M}$, where $\mathbf{A} \in \mathbb{R}^{K \times M}$ is the matrix with columns $(\mathbf{a}_1 - \mathbf{a}_0), \dots, (\mathbf{a}_M - \mathbf{a}_0)$, has full row rank, i.e., $\text{rank}(\tilde{\mathbf{W}}\mathbf{A}) = d_Z$, or the same holds for $\mathbf{W}\mathbf{A}$.

Then the latent representation and the effects of the observed perturbation combinations relative to \mathbf{a}_0 (as captured by $\mathbf{W}\mathbf{A}$) are identifiable up to orthogonal transformation, i.e., there is an orthogonal matrix $\mathbf{O} \in O(d_Z)$ such that

$$\forall \mathbf{z} \in \mathbb{R}^{d_Z} : \quad \tilde{\mathbf{f}}^{-1} \circ \mathbf{f}(\mathbf{z}) = \mathbf{O}\mathbf{z}, \quad (4.2)$$

$$\tilde{\mathbf{W}}\mathbf{A} = \mathbf{O}\mathbf{W}\mathbf{A}. \quad (4.3)$$

Proof. Let p_e and \tilde{p}_e denote the densities of

$$\mathbf{Z}_e := \mathbf{Z} + \mathbf{W}\mathbf{a}_e \quad (\text{A.2})$$

and

$$\tilde{\mathbf{Z}}_e := \tilde{\mathbf{Z}} + \tilde{\mathbf{W}}\mathbf{a}_e, \quad (\text{A.3})$$

respectively. Due to (4.1), \mathbf{f} and $\tilde{\mathbf{f}}$ have the same image. Thus, by the invertibility assumption (i), the function $\mathbf{h} := \tilde{\mathbf{f}}^{-1} \circ \mathbf{f} : \mathbb{R}^{d_Z} \rightarrow \mathbb{R}^{d_Z}$ is a well-defined C^2 -diffeomorphism. The change of variable formula applied to

$$\tilde{\mathbf{Z}}_e \stackrel{d}{=} \mathbf{h}(\mathbf{Z}_e) \quad (\text{A.4})$$

then yields for all e and all \mathbf{z} :

$$p_e(\mathbf{z}) = \tilde{p}_e(\mathbf{h}(\mathbf{z})) |\det \mathbf{J}_{\mathbf{h}}(\mathbf{z})|, \quad (\text{A.5})$$

where $\mathbf{J}_{\mathbf{h}}(\mathbf{z})$ denotes the Jacobian of \mathbf{h} . By taking logarithms of (A.5) and contrasting domain e with a reference domain with $e = 0$, the determinant terms cancel and we obtain for all e and all \mathbf{z} :

$$\log p_e(\mathbf{z}) - \log p_0(\mathbf{z}) = \log \tilde{p}_e(\mathbf{h}(\mathbf{z})) - \log \tilde{p}_0(\mathbf{h}(\mathbf{z})). \quad (\text{A.6})$$

Next, denote the densities of \mathbf{Z} and $\tilde{\mathbf{Z}}$ by p and \tilde{p} , respectively. From (A.2) and (A.3) it then follows that, for all e and all \mathbf{z} , p_e and \tilde{p}_e can respectively be expressed in terms of p and \tilde{p} as follows:

$$p_e(\mathbf{z}) = p(\mathbf{z} - \mathbf{W}\mathbf{a}_e), \quad (\text{A.7})$$

$$\tilde{p}_e(\mathbf{z}) = \tilde{p}(\mathbf{z} - \tilde{\mathbf{W}}\mathbf{a}_e). \quad (\text{A.8})$$

By substituting these expressions in (A.6), we obtain for all e and all \mathbf{z} :

$$\log p(\mathbf{z} - \mathbf{W}\mathbf{a}_e) - \log p(\mathbf{z} - \mathbf{W}\mathbf{a}_0) = \log \tilde{p}(\mathbf{h}(\mathbf{z}) - \tilde{\mathbf{W}}\mathbf{a}_e) - \log \tilde{p}(\mathbf{h}(\mathbf{z}) - \tilde{\mathbf{W}}\mathbf{a}_0). \quad (\text{A.9})$$

By the Gaussianity assumption (ii), the contrast of log-densities in (A.9) takes the following form for all e and all \mathbf{z} :

$$(\mathbf{a}_e - \mathbf{a}_0)^\top \mathbf{W}^\top (\mathbf{z} + \mathbf{W}\mathbf{a}_0) - \frac{1}{2}(\mathbf{a}_e - \mathbf{a}_0)^\top \mathbf{W}^\top \mathbf{W}(\mathbf{a}_e + \mathbf{a}_0) \quad (\text{A.10})$$

$$= (\mathbf{a}_e - \mathbf{a}_0)^\top \widetilde{\mathbf{W}}^\top (\mathbf{h}(\mathbf{z}) + \widetilde{\mathbf{W}}\mathbf{a}_0) - \frac{1}{2}(\mathbf{a}_e - \mathbf{a}_0)^\top \widetilde{\mathbf{W}}^\top \widetilde{\mathbf{W}}(\mathbf{a}_e + \mathbf{a}_0) \quad (\text{A.11})$$

We aim to show that the two representations are related by an affine transformation, i.e., that all second-order derivatives of \mathbf{h} are zero everywhere. Taking gradients w.r.t. \mathbf{z} yields for all e and all \mathbf{z} :

$$(\mathbf{a}_e - \mathbf{a}_0)^\top \mathbf{W}^\top = (\mathbf{a}_e - \mathbf{a}_0)^\top \widetilde{\mathbf{W}}^\top \mathbf{J}_h(\mathbf{z}). \quad (\text{A.12})$$

Let $\mathbf{A} \in \mathbb{R}^{K \times M}$ be the matrix with columns $\mathbf{a}_e - \mathbf{a}_0$ for $e \in [M]$. Then, for all \mathbf{z} :

$$\mathbf{A}^\top \mathbf{W}^\top = \mathbf{A}^\top \widetilde{\mathbf{W}}^\top \mathbf{J}_h(\mathbf{z}). \quad (\text{A.13})$$

Differentiating once more w.r.t. \mathbf{z} yields for all \mathbf{z} :

$$\mathbf{0} = \mathbf{A}^\top \widetilde{\mathbf{W}}^\top \mathbf{H}_h(\mathbf{z}), \quad (\text{A.14})$$

where the 3-tensor $\mathbf{H}_h(\mathbf{z}) \in \mathbb{R}^{d_Z \times d_Z \times d_Z}$ denotes the Hessian of \mathbf{h} , i.e., for all $i, j \in [d_Z]$ and all \mathbf{z}

$$\mathbf{0} = \mathbf{A}^\top \widetilde{\mathbf{W}}^\top \frac{\partial^2}{\partial z_i \partial z_j} \mathbf{h}(\mathbf{z}). \quad (\text{A.15})$$

By assumption (iii), the matrix $\mathbf{A}^\top \widetilde{\mathbf{W}}^\top$ has full column rank and thus a left inverse, i.e., there exists $\mathbf{V} \in \mathbb{R}^{d_Z \times M}$ such that $\mathbf{V} \mathbf{A}^\top \widetilde{\mathbf{W}}^\top = \mathbf{I}_{d_Z}$. Multiplying (A.15) on the left by \mathbf{V} then yields for all $i, j \in [d_Z]$ and all \mathbf{z} :

$$\frac{\partial^2}{\partial z_i \partial z_j} \mathbf{h}(\mathbf{z}) = \mathbf{0}. \quad (\text{A.16})$$

This implies that \mathbf{h} must be affine, i.e., there exist $\mathbf{M} \in \mathbb{R}^{d_Z \times d_Z}$ and $\mathbf{b} \in \mathbb{R}^{d_Z}$ such that for all \mathbf{z} :

$$\mathbf{h}(\mathbf{z}) = \mathbf{M}\mathbf{z} + \mathbf{b}. \quad (\text{A.17})$$

Further, since \mathbf{h} is invertible, \mathbf{M} must be invertible.

Recall that $\widetilde{\mathbf{Z}}_e \stackrel{d}{=} \mathbf{h}(\mathbf{Z}_e) = \mathbf{M}\mathbf{Z}_e + \mathbf{b}$. It follows from (A.2), (A.3) and assumption (ii) that for all $e \in [M]_0$:

$$\mathcal{N}\left(\widetilde{\mathbf{W}}(\mathbf{a}_e - \mathbf{a}_0), \mathbf{I}\right) = \mathcal{N}\left(\mathbf{M}\mathbf{W}(\mathbf{a}_e - \mathbf{a}_0) + \mathbf{b}, \mathbf{M}\mathbf{M}^\top\right). \quad (\text{A.18})$$

By equating the covariances, we find

$$\mathbf{M}\mathbf{M}^\top = \mathbf{I}, \quad (\text{A.19})$$

i.e., $\mathbf{M} = \mathbf{O}$ for some orthogonal matrix $\mathbf{O} \in O(d_Z)$.

Similarly, by equating the means, we obtain for all e :

$$\widetilde{\mathbf{W}}(\mathbf{a}_e - \mathbf{a}_0) = \mathbf{O}\mathbf{W}(\mathbf{a}_e - \mathbf{a}_0) + \mathbf{b} \quad (\text{A.20})$$

For $e = 0$, (A.20) yields

$$\mathbf{b} = \mathbf{0}. \quad (\text{A.21})$$

Stacking (A.20) for all other $e \in [M]$, we obtain

$$\widetilde{\mathbf{W}}\mathbf{A} = \mathbf{OWA}. \quad (\text{A.22})$$

This completes the proof. \square

A.3 Proof of Cor. 4.2

Corollary 4.2. *If, in addition to the assumptions of Thm. 4.1, $\mathbf{A} \in \mathbb{R}^{K \times M}$ has full row rank (i.e., $\text{rank}(\mathbf{A}) = K \leq M$), then the perturbation matrix \mathbf{W} is identifiable up to orthogonal transformation, i.e., $\widetilde{\mathbf{W}} = \mathbf{OW}$, where $\mathbf{O} \in O(d_Z)$ is an orthogonal matrix.*

Proof. If $\text{rank}(\mathbf{A}) = K$, then \mathbf{A} has a right inverse, i.e., there exists $\mathbf{K} \in \mathbb{R}^{M \times K}$ such that $\mathbf{AK} = \mathbf{I}_K$. Right multiplication of (A.22) by \mathbf{K} then yields

$$\widetilde{\mathbf{W}} = \mathbf{OW}. \quad (\text{A.23})$$

\square

A.4 Proof of Thm. 4.7

Theorem 4.7 (Extrapolation to span of relative perturbations). *Under the same setting and assumptions as in Thm. 4.1, let $\mathbf{a}_{\text{test}} \in \mathbb{R}^K$ be an unseen perturbation s.t.*

$$(\mathbf{a}_{\text{test}} - \mathbf{a}_0) \in \text{span}(\{\mathbf{a}_e - \mathbf{a}_0\}_{e \in [M]}). \quad (\text{4.5})$$

Then the effect of \mathbf{a}_{test} is uniquely identifiable in that

$$\mathbf{X}_{\text{test}} = \mathbf{f}(\mathbf{Z} + \mathbf{W}\mathbf{a}_{\text{test}}) \stackrel{d}{=} \widetilde{\mathbf{f}}(\widetilde{\mathbf{Z}} + \widetilde{\mathbf{W}}\mathbf{a}_{\text{test}}) \quad (\text{4.6})$$

Proof. With $\mathbf{h} = \widetilde{\mathbf{f}}^{-1} \circ \mathbf{f}$, the condition in (4.6) is equivalent to

$$\mathbf{h}(\mathbf{Z} + \mathbf{W}\mathbf{a}_{\text{test}}) \stackrel{d}{=} \widetilde{\mathbf{Z}} + \widetilde{\mathbf{W}}\mathbf{a}_{\text{test}}. \quad (\text{A.24})$$

By Thm. 4.1, we have $\mathbf{h}(\mathbf{z}) = \mathbf{O}\mathbf{z}$ for some orthogonal matrix $\mathbf{O} \in O(d_Z)$.

Together with $\mathbf{Z} \sim \mathcal{N}(-\mathbf{W}\mathbf{a}_0, \mathbf{I})$, this lets us compute the distribution of the LHS of (A.24) as:

$$\mathbf{h}(\mathbf{Z} + \mathbf{W}\mathbf{a}_{\text{test}}) = \mathbf{O}(\mathbf{Z} + \mathbf{W}\mathbf{a}_{\text{test}}) \sim \mathcal{N}(-\mathbf{OW}\mathbf{a}_0 + \mathbf{OW}\mathbf{a}_{\text{test}}, \mathbf{I}). \quad (\text{A.25})$$

Similarly, since $\widetilde{\mathbf{Z}} \sim \mathcal{N}(-\widetilde{\mathbf{W}}\mathbf{a}_0, \mathbf{I})$, the distribution of the RHS of (A.24) is given by

$$\widetilde{\mathbf{Z}} + \widetilde{\mathbf{W}}\mathbf{a}_{\text{test}} \sim \mathcal{N}(-\widetilde{\mathbf{W}}\mathbf{a}_0 + \widetilde{\mathbf{W}}\mathbf{a}_{\text{test}}, \mathbf{I}). \quad (\text{A.26})$$

To complete the proof, it thus remains to show that the means of (A.25) and (A.26) are equal, i.e.,

$$\mathbf{OW}(\mathbf{a}_{\text{test}} - \mathbf{a}_0) = \widetilde{\mathbf{W}}(\mathbf{a}_{\text{test}} - \mathbf{a}_0) \quad (\text{A.27})$$

Next, by (4.5), i.e., the assumption that $(\mathbf{a}_{\text{test}} - \mathbf{a}_0)$ lies in the span of $\{\mathbf{a}_e - \mathbf{a}_0\}_{e \in [M]}$, there exists $\boldsymbol{\alpha} \in \mathbb{R}^M$ such that

$$\mathbf{a}_{\text{test}} - \mathbf{a}_0 = \sum_{e \in [M]} \alpha_e (\mathbf{a}_e - \mathbf{a}_0) = \mathbf{A}\boldsymbol{\alpha} \quad (\text{A.28})$$

where, as before, $\mathbf{A} \in \mathbb{R}^{K \times M}$ is the matrix with columns $(\mathbf{a}_e - \mathbf{a}_0)$. Substituting (A.28) into (A.27) yields

$$\mathbf{OW}\mathbf{A}\boldsymbol{\alpha} = \widetilde{\mathbf{W}}\mathbf{A}\boldsymbol{\alpha} \quad (\text{A.29})$$

Finally, it follows from Thm. 4.1 that

$$OWA = \widetilde{W}A. \quad (\text{A.30})$$

which upon substitution into (A.29) completes the proof. \square

A.5 Proof of Prop. 4.9

Proposition 4.9 (Modeling shift interventions in SEMs). *Consider a linear SEM, $Z := B^\top Z + \eta$, with noise $\eta \sim \mathbb{P}_\eta$ and $B \in \mathbb{R}^{dz \times dz}$ a weighted adjacency matrix with spectral radius (largest absolute eigenvalue) $\rho(B) < 1$. Then, the distribution induced by shift interventions $a_e \in \mathbb{R}^{dz}$,*

$$Z := B^\top Z + \eta + a_e, \quad (\text{4.7})$$

is identical to that induced by (3.1) with $W = (I - B^\top)^{-1}$ and basal state distribution $\mathbb{P}_Z = (I - B^\top)_\#^{-1} \mathbb{P}_\eta$.

Proof. The distribution of Z induced by the SEM is most easily understood via the *reduced form* expression

$$Z = (I - B^\top)^{-1} \eta \quad (\text{A.31})$$

where the inverse $(I - B^\top)^{-1}$ exists since, by assumption, $\rho(B) < 1$. The observational (unintervened) distribution is thus given by $\mathbb{P}_Z = (I - B^\top)_\#^{-1} \mathbb{P}_\eta$. Now consider the shift interventions from (4.7). Analogous to (A.31), the reduced form of (4.7) is given by

$$Z = (I - B^\top)^{-1} \eta + (I - B^\top)^{-1} a_e. \quad (\text{A.32})$$

which is equal in distribution to

$$Z^{\text{pert}} = Z^{\text{base}} + W a_e \quad (\text{A.33})$$

with $Z^{\text{base}} \sim \mathbb{P}_Z = (I - B^\top)_\#^{-1} \mathbb{P}_\eta$ and $W = (I - B^\top)^{-1}$. \square

Remark A.2. The correspondence between mean shift perturbations and shift interventions appears to only hold for *linear* SCMs (at least in this simple form). Consider, for example, a nonlinear additive noise model,

$$Z := f(Z) + \eta, \quad (\text{A.34})$$

with reduced form given by $Z = g(\eta)$, where g is the inverse of the mapping $z \mapsto z - f(z)$. For shift interventions in (A.34) to match our perturbation model, we then must have

$$Z_e = g(\eta + a_e) = g(g^{-1}(Z) + a_e) = \phi(Z, a_e) \quad (\text{A.35})$$

for suitable ϕ and a_e . Thus, if f is nonlinear, so is g and this implies under weak assumptions that ϕ is nonlinear, too. In this case, shift interventions in a nonlinear SCM do not, in general, amount to mean shift perturbations (i.e., linear ϕ).

B PDAE training: Additional losses and complete algorithm

In this appendix, we discuss additional loss components (other than the perturbation loss from the main text), which are not required based on our theoretical results, but which may still benefit empirical performance, see Fig. 5 for an illustration.

Reconstructions. When considering the synthetic observations from (5.3) for $h = e$, i.e., when evaluated on the estimated perturbed latents from (5.1), we refer to the corresponding (random) decoder outputs as *reconstructions*,

$$\widehat{X}_{e,i} = \widehat{f}(\widehat{z}_{e,i}^{\text{pert}}, \varepsilon) \quad \text{where} \quad \varepsilon \sim \mathbb{Q}_\varepsilon. \quad (\text{B.1})$$

Conditional distribution over reconstructions. For any given observation x , we can sample reconstructions from the stochastic decoder by fixing its first argument to the encoding $\widehat{g}(x)$ and sampling noise from \mathbb{Q}_ε as in (B.1). Together, the encoder, decoder, and noise distribution thus induce a distribution over reconstructions, formally given by the push-forward

$$\widehat{f}(\widehat{g}(x), \cdot)_\# \mathbb{Q}_\varepsilon. \quad (\text{B.2})$$

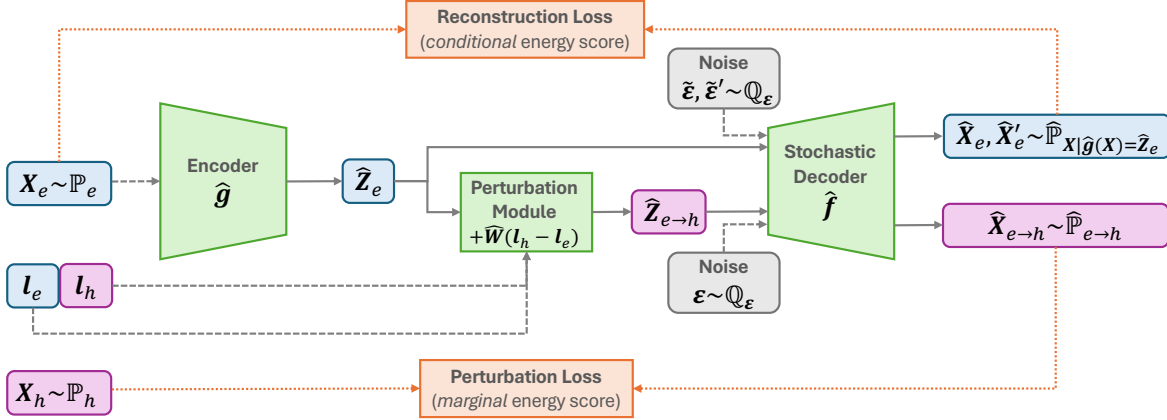


Figure 5. Extended illustration of the PDAE architecture including the reconstruction loss.

Since this distribution should ideally match that of $\mathbf{X}|\hat{g}(\mathbf{X}) = \hat{g}(\mathbf{x})$ (i.e., the true distribution of observations that share the same encoding),³ we denote it by $\hat{\mathbb{P}}_{\mathbf{X}|\hat{g}(\mathbf{X}) = \hat{g}(\mathbf{x})}$. Note that the first argument of \hat{f} in (B.2) is considered fixed, and all stochasticity stems from the noise ε . This contrasts with the simulated perturbed distributions $\mathbb{P}_{e \rightarrow h}$ in (5.4), where both \mathbf{X}_e and ε are random.

Conditional reconstruction loss. The conditional reconstruction loss $\mathcal{L}_{\text{cond-rec}}$ is given by the sum of domain-specific DPA losses (Shen & Meinshausen, 2024a),

$$\mathcal{L}_{\text{cond-rec}}\left(\widehat{\mathbf{g}}, \widehat{\mathbf{f}}; \{\mathbb{P}_e\}_{e \in [M]_0}\right) := \sum_{e \in [M]_0} -\mathbb{E}_{\mathbf{X}_e \sim \mathbb{P}_e} \left[\text{ES}_\beta\left(\widehat{\mathbb{P}}_{\mathbf{X}|\widehat{\mathbf{g}}(\mathbf{X})=\widehat{\mathbf{g}}(\mathbf{X}_e)}, \mathbf{X}_e\right) \right], \quad (\text{B.3})$$

where each summand on the RHS of (B.3) involves a *conditional* energy score (i.e., one whose first argument also depends on X_e), see § C.3 for further discussion. It should be noted that the pairwise sum in the perturbation loss of (5.5) also includes the case $h = e$. Enforcing $\mathbb{P}_e = \widehat{\mathbb{P}}_{e \rightarrow e}$ can be viewed as a marginal reconstruction objective and thus as a weaker constraint than that enforced by $\mathcal{L}_{\text{cond-rec}}$.

Prior loss. To turn PDAE into a full generative model and remove unnecessary ambiguities from the learned representation, we propose an additional loss which quantifies deviations of the encoded latent basal state distributions from a fixed Gaussian prior. Since, by Lemma A.1, the prior mean and covariance are arbitrary, we choose $\mathbb{P}^{\text{base}} = \mathcal{N}(\mathbf{0}, \mathbf{I})$ for convenience. Denote by $\widehat{\mathbb{P}}_{\widehat{\mathbf{g}}(\mathbf{X}_e) - \mathbf{W}\mathbf{a}_e}$ the distribution of

$$\widehat{g}(X_e) - \widehat{W}a_e, \quad \text{where} \quad X_e \sim \mathbb{P}_e. \quad (\text{B.4})$$

We then define the prior loss as the sum over domains of the negative expected energy score between the true fixed prior and the encoded basal state distribution from domain e ,

$$\mathcal{L}_{\text{prior}}\left(\widehat{\mathbf{g}}, \widehat{\mathbf{W}}; \left\{(\mathbb{P}_e, \mathbf{a}_e)\right\}_{e=0}^M\right) := \sum_{e \in [M]_0} -\mathbb{E}_{\mathbf{Z}^{\text{base}} \sim \mathbb{P}^{\text{base}}} \left[\text{ES}_{\beta}\left(\widehat{\mathbb{P}}_{\widehat{\mathbf{g}}(\mathbf{X}_e) - \widehat{\mathbf{W}}\mathbf{a}_e}, \mathbf{Z}^{\text{base}}\right) \right]. \quad (\text{B.5})$$

In practice, the prior loss can be approximated using the estimated latent basal states,

$$\hat{z}_{e,i}^{\text{base}} := \hat{z}_{e,i}^{\text{pert}} - \hat{W}a_e = \hat{g}(x_{e,i}) - \hat{W}a_e \quad (\text{B.6})$$

Sparsity. Similar to Bereket & Karaletsos (2023), we also consider a sparsity penalty $\|\widehat{\mathbf{W}}\|_{2,1}$ on the inferred $\widehat{\mathbf{W}}$.

³For example, if $\hat{\mathbf{g}}$ is injective, the true reconstruction distribution is a point mass on \mathbf{x} , whereas if $\hat{\mathbf{g}}$ is constant, it is the full (unconditional) distribution of \mathbf{X} . In this sense, the distribution of reconstructions captures the information about \mathbf{x} that is left unexplained given only its encoding (Shen & Meinshausen, 2024a).

Combined loss. Given loss weight hyperparameters $(\lambda_R, \lambda_{\text{prior}}, \lambda_S)$ and denoting the perturbation loss from (5.5) by $\mathcal{L}_{\text{pert}}(\hat{\mathbf{g}}, \hat{\mathbf{f}}, \hat{\mathbf{W}}; \{(\mathbb{P}_e, \mathbf{a}_e)\}_{e=0}^M)$ we can then combine the different losses into one objective as follows:

$$\begin{aligned} (\hat{\mathbf{g}}^*, \hat{\mathbf{f}}^*, \hat{\mathbf{W}}^*) &\in \arg \min_{\hat{\mathbf{g}}, \hat{\mathbf{f}}, \hat{\mathbf{W}}} \mathcal{L}_{\text{pert}}(\hat{\mathbf{g}}, \hat{\mathbf{f}}, \hat{\mathbf{W}}; \{(\mathbb{P}_e, \mathbf{a}_e)\}_{e=0}^M) + \lambda_R \mathcal{L}_{\text{cond-rec}}(\hat{\mathbf{g}}, \hat{\mathbf{f}}; \{\mathbb{P}_e\}_{e=0}^M) \\ &\quad + \lambda_{\text{prior}} \mathcal{L}_{\text{prior}}(\hat{\mathbf{g}}, \hat{\mathbf{W}}; \{(\mathbb{P}_e, \mathbf{a}_e)\}_{e=0}^M) + \lambda_S \|\hat{\mathbf{W}}\|_{2,1}. \end{aligned} \quad (\text{B.7})$$

To avoid that the encoder captures latent dimensions of maximal variation as in DPA (Shen & Meinshausen, 2024a) rather than focus on the perturbation-relevant latents Z , we do not update the encoder parameters using the reconstruction loss.

Algorithm. The complete algorithm for one training iteration for PDAE is provided in Alg. 1.

Algorithm 1 PDAE training step

Require: mini-batch $\{(\mathbf{x}_i, \mathbf{a}_i)\}_{i=1}^B$, model $(\hat{\mathbf{g}}_\phi, \hat{\mathbf{f}}_\theta, \hat{\mathbf{W}})$, learning rates $(\eta_\theta, \eta_\phi, \eta_w)$, loss weights $(\lambda_R, \lambda_{\text{prior}}, \lambda_S)$

1: $\mathcal{L}_{\text{cond-rec}}(\phi, \theta), \mathcal{L}_{\text{pert}}(\phi, \theta, \hat{\mathbf{W}}) \leftarrow 0, 0$ # initialize losses

2: **for** $i = 1, \dots, B$ **do**

3: $\hat{\mathbf{z}}_i^{\text{pert}} \leftarrow \hat{\mathbf{g}}_\phi(\mathbf{x}_i)$ # encode

4: $\boldsymbol{\varepsilon}_i, \boldsymbol{\varepsilon}'_i \sim \mathcal{N}(\mathbf{0}, \mathbf{I})$ # noise for reconstructions

5: $\hat{\mathbf{x}}_i, \hat{\mathbf{x}}'_i \leftarrow \hat{\mathbf{f}}_\theta(\hat{\mathbf{z}}_i^{\text{pert}}, \boldsymbol{\varepsilon}_i), \hat{\mathbf{f}}_\theta(\hat{\mathbf{z}}_i^{\text{pert}}, \boldsymbol{\varepsilon}'_i)$ # noisy reconstructions

6: $\mathcal{L}_{\text{cond-rec}}(\phi, \theta) += \frac{1}{2B} (\|\mathbf{x}_i - \hat{\mathbf{x}}_i\| + \|\mathbf{x}_i - \hat{\mathbf{x}}'_i\| - \|\hat{\mathbf{x}}_i - \hat{\mathbf{x}}'_i\|)$ # conditional energy score

7: $\hat{\mathbf{z}}_i^{\text{base}} \leftarrow \hat{\mathbf{z}}_i^{\text{pert}} - \hat{\mathbf{W}} \mathbf{a}_i$ # estimated basal states

8: **for** $j \in [B] \setminus \{i\}$ **do**

9: $\hat{\mathbf{z}}_{j \rightarrow i}^{\text{pert}} \leftarrow \hat{\mathbf{z}}_j^{\text{base}} + \hat{\mathbf{W}} \mathbf{a}_i$ # synthetic perturbed latents

10: $\boldsymbol{\varepsilon}_{ji} \sim \mathcal{N}(\mathbf{0}, \mathbf{I})$ # noise for synthetic observations

11: $\hat{\mathbf{x}}_{j \rightarrow i} \leftarrow \hat{\mathbf{f}}_\theta(\hat{\mathbf{z}}_{j \rightarrow i}^{\text{pert}}, \boldsymbol{\varepsilon}_{ji})$ # synthetic observations

12: **end for**

13: $\mathcal{L}_{\text{pert}}(\phi, \theta, \hat{\mathbf{W}}) += \frac{1}{B(B-1)} \sum_{j \in [B] \setminus \{i\}} \left[\|\mathbf{x}_i - \hat{\mathbf{x}}_{j \rightarrow i}\| - \frac{1}{B-2} \sum_{i \neq j' < j} \|\hat{\mathbf{x}}_{j \rightarrow i} - \hat{\mathbf{x}}_{j' \rightarrow i}\| \right]$

14: $\boldsymbol{\xi}_i \sim \mathcal{N}(\mathbf{0}, \mathbf{I})$ # noise for prior loss

15: **end for**

16: $\mathcal{L}_{\text{prior}}(\phi, \hat{\mathbf{W}}) \leftarrow \frac{1}{B^2} \sum_{i, j \in [B]} \|\boldsymbol{\xi}_i - \hat{\mathbf{z}}_j^{\text{base}}\| - \frac{1}{B(B-1)} \sum_{j' < j \in [B]} \|\hat{\mathbf{z}}_j^{\text{base}} - \hat{\mathbf{z}}_{j'}^{\text{base}}\|$ # marginal energy score

17: $\theta \leftarrow \theta - \eta_\theta \nabla_\theta (\mathcal{L}_{\text{pert}}(\phi, \theta, \hat{\mathbf{W}}) + \lambda_R \mathcal{L}_{\text{cond-rec}}(\phi, \theta))$ # update decoder

18: $\phi \leftarrow \phi - \eta_\phi \nabla_\phi (\mathcal{L}_{\text{pert}}(\phi, \theta, \hat{\mathbf{W}}) + \lambda_{\text{prior}} \mathcal{L}_{\text{prior}}(\phi, \hat{\mathbf{W}}))$ # update encoder

19: $\hat{\mathbf{W}} \leftarrow \hat{\mathbf{W}} - \eta_w \nabla_{\hat{\mathbf{W}}} (\mathcal{L}_{\text{pert}}(\phi, \theta, \hat{\mathbf{W}}) + \lambda_{\text{prior}} \mathcal{L}_{\text{prior}}(\phi, \hat{\mathbf{W}}) + \lambda_S \|\hat{\mathbf{W}}\|_{2,1})$ # update perturbation matrix

MMD-based goodness of fit assessment. To assess goodness of fit (e.g., for early stopping or to assess training convergence), we propose to assess the pairwise distributional fits between simulated and true perturbation distributions using MMD. That is, to consider $\text{MMD}(\mathbb{P}_{e \rightarrow h}, \mathbb{P}_e)$ for all $e, h \in [M]_0$.

Code. We will publicly release PDAE code upon publication.

C Additional background material and related work

Since the problem of interest (§ 2) involves making distributional predictions for new perturbation conditions, we review some basics of probabilistic forecasting (§ C.1) and measuring the similarity between two distributions (§ C.2), in our case typically between an empirical distribution and its predicted counterpart. We then turn to representation learning with encoder-decoder architectures (§ C.3), in particular a recent approach that also targets distributional reconstruction. Finally, we cover some prior efforts on perturbation modeling and extrapolation (§ C.4), which we draw inspiration from.

C.1 Probabilistic forecasting and scoring rules

Let Ω be a sample space, \mathcal{A} a σ -algebra of subsets of Ω , and \mathcal{P} a convex class of probability measures on (Ω, \mathcal{A}) . A *probabilistic prediction* or *probabilistic forecast* is a mapping into \mathcal{P} , which outputs predictive distributions \mathbb{P} over outcomes $x \in \Omega$. Probabilistic forecasting can thus be viewed as a distributional generalization point prediction (i.e., deterministic forecasting), which maps directly into Ω .

To evaluate, compare, or rank different forecasts, it is useful to assign them a numerical score reflecting their quality. A *scoring rule* is a function $S : \mathcal{P} \times \Omega \rightarrow \mathbb{R}$ that assigns a score $S(\mathbb{P}, x)$ to forecast \mathbb{P} if event x materializes, with higher scores corresponding to better forecasts—akin to (negative) loss or cost functions for point predictions. If x is distributed according to \mathbb{Q} , we denote the *expected score* by $S(\mathbb{P}, \mathbb{Q}) = \mathbb{E}_{x \sim \mathbb{Q}}[S(\mathbb{P}, x)]$. The scoring rule is called *proper* if $S(\mathbb{Q}, \mathbb{Q}) \geq S(\mathbb{P}, \mathbb{Q})$ for all \mathbb{P} , and *strictly proper* if equality holds if and only if $\mathbb{P} = \mathbb{Q}$.

CRPS. For continuous scalar random variables (i.e., $\Omega = \mathbb{R}$), a popular scoring rule is the *continuous ranked probability score* (CRPS; Matheson & Winkler, 1976). When \mathcal{P} is the space of Borel probability measures on \mathbb{R} with finite first moment, it is strictly proper and given by:⁴

$$\text{CRPS}(\mathbb{P}, x) = \frac{1}{2} \mathbb{E}_{X, X' \stackrel{\text{i.i.d.}}{\sim} \mathbb{P}} |X - X'| - \mathbb{E}_{X \sim \mathbb{P}} |X - x|. \quad (\text{C.1})$$

If \mathbb{P} is a point mass, the negative CRPS reduces to the absolute error loss function; it can thus be viewed as a generalization thereof to probabilistic forecasts.

Energy score. Gneiting & Raftery (2007) propose the *energy score* as a multi-variate generalization of the CRPS for vector-valued $\mathbf{x} \in \Omega = \mathbb{R}^{d_x}$. For $\beta \in (0, 2)$, it is defined by

$$\text{ES}_\beta(\mathbb{P}, \mathbf{x}) = \frac{1}{2} \mathbb{E}_{\mathbf{X}, \mathbf{X}' \stackrel{\text{i.i.d.}}{\sim} \mathbb{P}} \|\mathbf{X} - \mathbf{X}'\|_2^\beta - \mathbb{E}_{\mathbf{X} \sim \mathbb{P}} \|\mathbf{X} - \mathbf{x}\|_2^\beta, \quad (\text{C.2})$$

where $\|\cdot\|_2$ denotes the Euclidean (L2) norm. ES_β is strictly proper w.r.t. \mathcal{P}_β , the set of Borel probability measures \mathbb{P} for which $\mathbb{E}_{\mathbf{X} \sim \mathbb{P}} \|\mathbf{X}\|_2^\beta$ is finite (Gneiting & Raftery, 2007).

C.2 Assessing distributional similarity

Energy distance. The expected energy score $\text{ES}_\beta(\mathbb{P}, \mathbb{Q}) = \mathbb{E}_{\mathbf{Y} \sim \mathbb{Q}}[\text{ES}_\beta(\mathbb{P}, \mathbf{Y})]$ constitutes a measure of similarity between \mathbb{P} and \mathbb{Q} and is closely linked to the *energy distance* (Székely & Rizzo, 2013):

$$\text{ED}_\beta(\mathbb{P}, \mathbb{Q}) = 2\mathbb{E}_{\mathbf{X} \sim \mathbb{P}, \mathbf{Y} \sim \mathbb{Q}} \|\mathbf{X} - \mathbf{Y}\|_2^\beta - \mathbb{E}_{\mathbf{X}, \mathbf{X}' \stackrel{\text{i.i.d.}}{\sim} \mathbb{P}} \|\mathbf{X} - \mathbf{X}'\|_2^\beta - \mathbb{E}_{\mathbf{Y}, \mathbf{Y}' \stackrel{\text{i.i.d.}}{\sim} \mathbb{Q}} \|\mathbf{Y} - \mathbf{Y}'\|_2^\beta \quad (\text{C.3})$$

$$= 2(\text{ES}_\beta(\mathbb{Q}, \mathbb{Q}) - \text{ES}_\beta(\mathbb{P}, \mathbb{Q})) \geq 0 \quad (\text{C.4})$$

with equality if and only if $\mathbb{P} = \mathbb{Q}$, since ES_β is a strictly proper scoring rule.

Maximum mean discrepancy (MMD). Another well-known distance between probability measures that is rooted in kernel methods (Schölkopf & Smola, 2002) is the *maximum mean discrepancy* (MMD; Gretton et al., 2012), which for a positive definite kernel $k : \Omega \times \Omega \rightarrow \mathbb{R}$ is given by

$$\text{MMD}_k^2(\mathbb{P}, \mathbb{Q}) = \mathbb{E}_{X, X' \stackrel{\text{i.i.d.}}{\sim} \mathbb{P}} [k(X, X')] - 2\mathbb{E}_{X \sim \mathbb{P}, Y \sim \mathbb{Q}} [k(X, Y)] + \mathbb{E}_{Y, Y' \stackrel{\text{i.i.d.}}{\sim} \mathbb{Q}} [k(Y, Y')]. \quad (\text{C.5})$$

⁴The original definition by Matheson & Winkler (1976) is $\text{CRPS}(\mathbb{P}, x) = -\int_{-\infty}^{\infty} (F(y) - 1\{y \geq x\})^2 dy$ where F is the CDF of \mathbb{P} , but the simpler form in (C.1) has been shown to be equivalent (Baringhaus & Franz, 2004, Lemma 2.2).

Energy distance as a special case of MMD. As shown by Sejdinovic et al. (2013), if k in (C.5) is chosen to be the positive-definite *distance kernel*⁵

$$k_\beta(\mathbf{X}, \mathbf{Y}) = \frac{1}{2} \left(\|\mathbf{X}\|_2^\beta + \|\mathbf{Y}\|_2^\beta - \|\mathbf{X} - \mathbf{Y}\|_2^\beta \right) \quad (\text{C.6})$$

then the energy distance is recovered as a special case of MMD,

$$\text{ED}_\beta(\mathbb{P}, \mathbb{Q}) = 2 \text{MMD}_{k_\beta}^2(\mathbb{P}, \mathbb{Q}). \quad (\text{C.7})$$

C.3 Representation learning

Many modern data sources of interest contain high-dimensional and unstructured observations \mathbf{x} , such as audio, video, images, or text. Representation learning aims to transform such data into a more compact, lower-dimensional set of features \mathbf{z} (the representation) which preserves most of the relevant information while making it more easily accessible, e.g., for use in downstream tasks (Bengio et al., 2013).⁶ For example, a representation of images of multi-object scenes could be a list of the contained objects, along with their size, position, colour, etc. A key assumption underlying this endeavour is the so-called *manifold hypothesis* which posits that high-dimensional natural data tends to lie near a low-dimensional manifold embedded in the high-dimensional ambient space; this idea is also at the heart of several (nonlinear) dimension reduction techniques (Cayton, 2005; Tenenbaum et al., 2000; Saul & Roweis, 2003; Belkin & Niyogi, 2001).

Autoencoder (AE). An autoencoder (AE; Hinton & Salakhutdinov, 2006; Rumelhart et al., 1986) is a pair of functions (\mathbf{g}, \mathbf{f}) , consisting of an *encoder* $\mathbf{g} : \mathbb{R}^{d_X} \rightarrow \mathbb{R}^{d_Z}$ mapping observations $\mathbf{X} \sim \mathbb{P}$ to their representation $\mathbf{Z} := \mathbf{g}(\mathbf{X})$, and a *decoder* $\mathbf{f} : \mathbb{R}^{d_Z} \rightarrow \mathbb{R}^{d_X}$ mapping representations \mathbf{Z} to their reconstructions in observation space, $\widehat{\mathbf{X}} := \mathbf{f}(\mathbf{Z}) = \mathbf{f}(\mathbf{g}(\mathbf{X}))$. Typically, $d_Z < d_X$, such that there is a bottleneck and perfect reconstruction is not feasible. Autoencoders are usually trained with a (point-wise, mean) reconstruction objective, i.e., the aim is to minimise the mean squared error

$$\mathcal{L}_{\text{AE}}(\mathbf{g}, \mathbf{f}; \mathbb{P}) := \mathbb{E}_{\mathbf{X} \sim \mathbb{P}} \left\| \mathbf{X} - \widehat{\mathbf{X}} \right\|_2^2 = \mathbb{E}_{\mathbf{X} \sim \mathbb{P}} \left\| \mathbf{X} - \mathbf{f}(\mathbf{g}(\mathbf{X})) \right\|_2^2, \quad (\text{C.8})$$

w.r.t. both \mathbf{g} and \mathbf{f} . As a result, the optimal decoder \mathbf{f}_{AE}^* for any fixed encoder choice \mathbf{g} is given by the conditional mean

$$\mathbf{f}_{\text{AE}}^*(\mathbf{z}; \mathbf{g}, \mathbb{P}) = \mathbb{E}_{\mathbf{X} \sim \mathbb{P}} [\mathbf{X} | \mathbf{g}(\mathbf{X}) = \mathbf{z}]. \quad (\text{C.9})$$

Distributional principal autoencoder (DPA). Since the objective of a standard AE is mean reconstruction, the distribution of reconstructions $\widehat{\mathbf{X}}$ is typically not the same as the distribution of \mathbf{X} (unless the encoder is invertible, i.e, the compression is lossless and perfect reconstruction is feasible, which is usually not the case in practice). To address this, Shen & Meinshausen (2024a) proposed the distributional principal autoencoder (DPA) which targets distributional (rather than mean) reconstruction. A DPA also consists of an encoder-decoder pair (\mathbf{g}, \mathbf{f}) . However, unlike in a standard AE, the DPA decoder $\mathbf{f} : \mathbb{R}^{d_Z} \times \mathbb{R}^{d_\epsilon} \rightarrow \mathbb{R}^{d_X}$ is stochastic in that it receives an additional noise term ϵ as input, which is distributed according to a fixed distribution \mathbb{Q}_ϵ such as a standard isotropic Gaussian. The DPA loss function is constructed such that for a fixed encoder \mathbf{g} , the optimal DPA decoder $\mathbf{f}_{\text{DPA}}^*$ maps a given latent embedding \mathbf{z} to the distribution of \mathbf{X} , given $\mathbf{g}(\mathbf{X}) = \mathbf{z}$, i.e.,

$$\mathbf{f}_{\text{DPA}}^*(\mathbf{z}, \epsilon; \mathbf{g}) \stackrel{d}{=} (\mathbf{X} | \mathbf{g}(\mathbf{X}) = \mathbf{z}), \quad (\text{C.10})$$

where $\stackrel{d}{=}$ denotes equality in distribution. This means that the decoder evaluated at \mathbf{z} should match the distribution of all realizations of \mathbf{X} that are mapped by the encoder to \mathbf{z} . At the same time, the DPA encoder aims to minimise the variability in the distributions in (C.10) by encoding the first d_Z “principal” components. As shown by Shen & Meinshausen (2024a),

⁵induced by the negative-definite semi-metric $\rho(\mathbf{X}, \mathbf{Y}) = \|\mathbf{X} - \mathbf{Y}\|_2^\beta$ on $\Omega = \mathbb{R}^{d_X}$ (centered at the origin),

⁶Representation learning is thus closely related to the classical task of dimension reduction. The former usually refers to nonlinear settings, involves some form of machine learning, and tends to be more focused on usefulness in terms of downstream tasks, rather than, say, explained variance.

both of these goals are achieved by the following DPA objective,

$$\begin{aligned}\mathcal{L}_{\text{DPA}}(\mathbf{g}, \mathbf{f}; \mathbb{P}) &= \mathbb{E}_{\mathbf{X} \sim \mathbb{P}, \varepsilon \sim \mathbb{Q}_\varepsilon} \|\mathbf{X} - \mathbf{f}(\mathbf{g}(\mathbf{X}), \varepsilon)\|_2^\beta - \frac{1}{2} \mathbb{E}_{\mathbf{X} \sim \mathbb{P}, \varepsilon, \varepsilon' \stackrel{\text{iid}}{\sim} \mathbb{Q}_\varepsilon} \|\mathbf{f}(\mathbf{g}(\mathbf{X}), \varepsilon) - \mathbf{f}(\mathbf{g}(\mathbf{X}), \varepsilon')\|_2^\beta \\ &= -\mathbb{E}_{\mathbf{X} \sim \mathbb{P}} \left[\text{ES}_\beta \left(\mathbf{f}(\mathbf{g}(\mathbf{X}), \cdot) \# \mathbb{Q}_\varepsilon, \mathbf{X} \right) \right],\end{aligned}\quad (\text{C.11})$$

where $\mathbf{f}(z, \cdot) \# \mathbb{Q}_\varepsilon$ denotes the pushforward distribution of \mathbb{Q}_ε through the function $\mathbf{f}(z, \cdot)$, i.e., the distribution of $\mathbf{f}(z, \varepsilon)$ for a fixed z when $\varepsilon \sim \mathbb{Q}_\varepsilon$. In other words, a DPA minimizes the negative expected energy score between \mathbf{X} and the corresponding (stochastic) decoder output, conditional on the encoding of \mathbf{X} . Due to this conditioning, the DPA objective differs from an energy distance by a “normalization constant” which depends on the encoder and encourages capturing principal (i.e., variation-minimizing) components, rather than random latent dimensions.

C.4 Perturbation modeling

Compositional perturbation autoencoder (CPA). [Lotfollahi et al. \(2023\)](#) propose the compositional perturbation autoencoder (CPA) as a model for compositional extrapolation of perturbation data. Specifically, they assume the following model:

$$\mathbf{z}^{\text{pert}} = \mathbf{z}^{\text{base}} + \mathbf{W}^{\text{pert}} \begin{pmatrix} h_1(a_1) \\ \vdots \\ h_K(a_K) \end{pmatrix} + \sum_{j=1}^J \mathbf{W}_j^{\text{cov}} \mathbf{c}_j, \quad (\text{C.12})$$

where $\mathbf{z}^{\text{base}} \sim \mathbb{P}_Z$ denotes an unperturbed basal state; the matrix $\mathbf{W}^{\text{pert}} \in \mathbb{R}^{d_Z \times K}$ encodes the additive effect of each elementary perturbation; $\{h_k : \mathbb{R} \rightarrow \mathbb{R}\}_{k \in [K]}$ are unknown, possibly nonlinear dose-response curves; $\{\mathbf{c}_j \in \mathbb{R}^{K_j}\}_{j \in [J]}$ are observed one-hot vectors capturing J additional discrete covariates, such as cell-types or species; and the matrices $\{\mathbf{W}_j^{\text{cov}} \in \mathbb{R}^{d_Z \times K_j}\}_{j \in [J]}$ encode additive covariate-specific effects. Further, the basal state \mathbf{z}^{base} is assumed to be independent of the perturbation labels \mathbf{a} and covariates $\mathbf{C} = (\mathbf{c}_1, \dots, \mathbf{c}_J)$. Observations \mathbf{x} are then drawn from a Gaussian whose mean and variance are determined by the perturbed latent state \mathbf{z}^{pert} ,

$$\mathbf{x} \sim \mathcal{N} \left(\mu(\mathbf{z}^{\text{pert}}), \sigma^2(\mathbf{z}^{\text{pert}}) \mathbf{I} \right). \quad (\text{C.13})$$

To fit this model, [Lotfollahi et al. \(2023\)](#) employ an adversarial autoencoder ([Lample et al., 2017](#)). First, an encoder \mathbf{g} estimates the basal state

$$\hat{\mathbf{z}}^{\text{base}} = \mathbf{g}(\mathbf{x}). \quad (\text{C.14})$$

The estimated perturbed latent state $\hat{\mathbf{z}}^{\text{pert}}$ is then computed according to (C.12) using (C.14) and learnt estimates $\hat{\mathbf{W}}^{\text{pert}}$, $\{\hat{h}_k\}$, and $\{\hat{\mathbf{W}}_l^{\text{cov}}\}$. Finally, a (deterministic) decoder \mathbf{f} uses $\hat{\mathbf{z}}^{\text{pert}}$ to compute estimates of the mean and variance in (C.13), i.e., $(\hat{\mu}, \hat{\sigma}^2) = \mathbf{f}(\hat{\mathbf{z}}^{\text{pert}})$. All learnable components of the model are trained by minimizing the (Gaussian) negative log-likelihood of the observed data $\mathcal{D} = \{(\mathbf{x}_i, \mathbf{a}_i, \mathbf{C}_i)\}_{i \in [N]}$. To encourage the postulated independence of $\hat{\mathbf{z}}^{\text{base}}$ and (\mathbf{a}, \mathbf{C}) , an additional adversarial loss is used, which minimizes the predictability of the latter from the former.

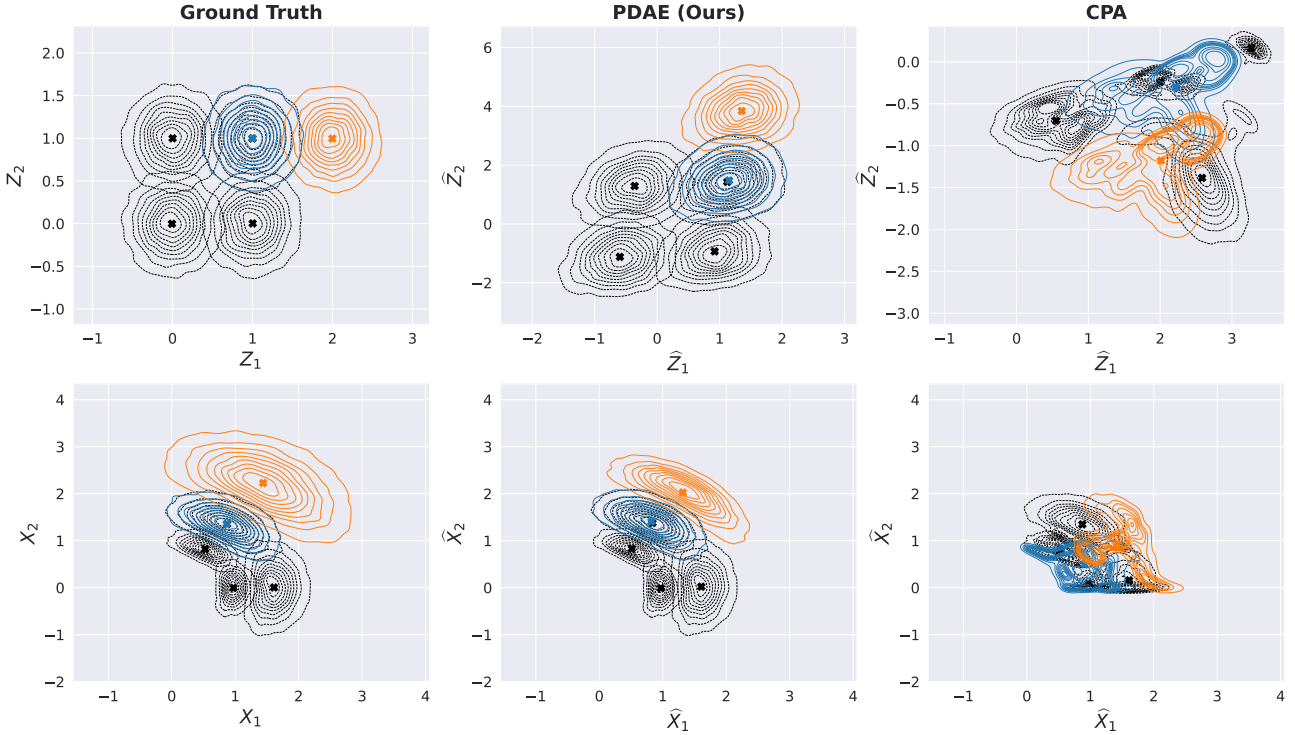


Figure 6. Qualitative comparison of PDAE and CPA on synthetic 2D data. Rows correspond to latent space (top) and observation space (bottom). Columns show the ground truth data (left), PDAE predictions (center), and CPA predictions (right). Training domains are shown in grey, an in-distribution (ID) test case with $\alpha_{\text{test}}^{\text{ID}} = (1, 1, 0)^\top$ (which overlaps with one of the training domains) in blue, and an out-of-distribution (OOD) test case with $\alpha_{\text{test}}^{\text{OOD}} = (1, 0, 1)^\top$ in orange. All plots show kernel density estimates of the distributions; crosses (x) indicate the corresponding means. As can be seen, PDAE recovers an affine transformation of the true latents (top, center) leading to accurate distributional predictions for the training and ID test domain (bottom, center). However, the OOD test domain is mapped to a part of the latent space not seen during training (top, center). As a result, the corresponding decoder output does not accurately match the true OOD distribution (bottom left vs center). CPA accurately predicts the means of the training distribution (bottom right, black crosses) but does not recover the true latents up to an affine transformation (top right). Moreover, the predicted distributions for CPA do not match the ground truth particularly well, particularly for the test conditions (bottom left vs right). However, recall that—unlike PDAE—CPA is not trained for distributional reconstruction, see § C.4 for details.

D Additional experimental details and results

D.1 Hyperparameter selection for CPA

For CPA, hyperparameters are chosen by randomly searching over a predefined parameter space for 100 trials for every dataset, see Tab. 1 of [Lotfollahi et al. \(2023\)](#) for details. To improve the CPA fit on our simulation data and render the comparison with PDAE fairer, we mimic this procedure and run a random search for 100 trials over a subset of these hyperparameters, which we show in Tab. 2. We tune all parameters that are neither linked to the architecture nor related to the non-linear dose-response functions. (In the setting of gene perturbation experiments that we emulate here, the dose responses are set to the identity, and thus no doser MLP hyperparameters are needed.) After randomly choosing 100 configurations of the parameter space and training a CPA model for 2000 epochs on each, we compute the MMD between predictions and ground truth of 7 ID evaluation environments and select the configuration that minimizes the MMD. The optimal configuration is shown in Tab. 2.

D.2 Robustness experiment with varying signal-to-noise ratio

In this experiment, each observation $x_{e,i}$ is generated from two signal dimensions $z_{e,i}^{\text{pert}} \in \mathbb{R}^2$ and eight noise dimensions $\varepsilon_{e,i}^{\text{pert}} \in \mathbb{R}^8$ as input for the nonlinear mixing function, as described at the end of § 7. We evaluate model robustness under increasing levels of noise by varying the standard deviation σ_ε of the noise variable $\varepsilon \sim \mathbb{Q}_\varepsilon$ in the data-generating process. The list of values of σ_ε considered is $[0, 0.1, 0.25, 0.5, 1, 2, 10]$. We choose the same hyperparameters as described in § 7, with the exception of increasing CPA’s bottleneck dimension to 10 and PDAE’s decoder model noise dimension to 8. Like

Table 2. Tuned Hyperparameters of CPA with their search space and optimal value. We sample 100 random configurations from the joint search space and train a CPA model for 2000 epochs for each. The optimal configuration minimizes the MMD on ID validation data.

Hyperparameter	Search Space	Selected Optimal Value
step_size_lr	$\{15, 25, 45\}$	15
autoencoder_lr	$10^{\mathcal{U}[-5, -2]}$	3.63×10^{-4}
autoencoder_wd	$10^{\mathcal{U}[-8, -4]}$	5.97×10^{-6}
reg_adversary	$10^{\mathcal{U}[-2, 2]}$	2.31×10^{-2}
penalty_adversary	$10^{\mathcal{U}[-2, 2]}$	8.15×10^{-2}
adversary_lr	$10^{\mathcal{U}[-5, -2]}$	1.7×10^{-4}
adversary_wd	$10^{\mathcal{U}[-8, -4]}$	3.11×10^{-6}
adversary_steps	$\{1, 2, 3, 4, 5\}$	5

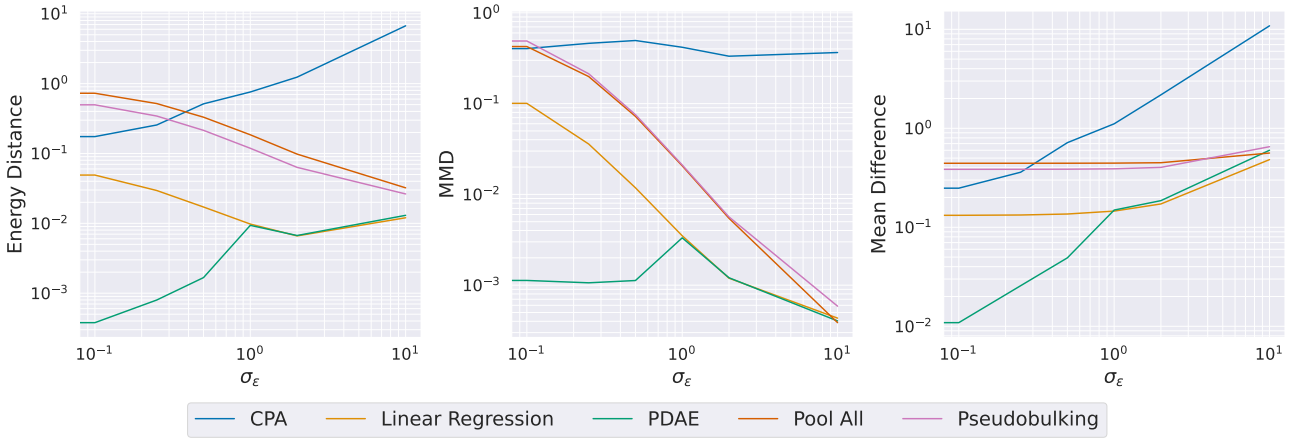


Figure 7. Evaluation of Robustness Under Increasing Levels of Noise. We compare the ID test performance of the baseline methods, CPA, and PDAE for higher dimensional observations with additional noise dimensions appended while increasing the level of noise σ_ε .

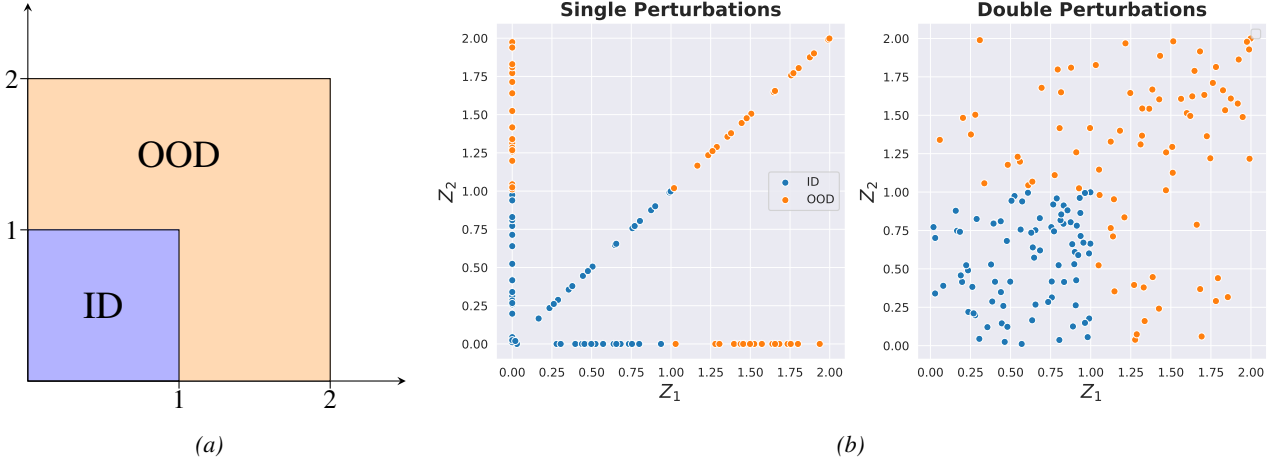


Figure 8. (a) **Sampling space for ID and OOD test cases.** Representation of the ID region (in blue) as defined by the elementary mean shifts in the perturbation matrix and a possible OOD region (in orange) for mean shifts in the Euclidean plane. (b) **Mean shifts of generated ID and OOD perturbation labels.** Mean shifts from single perturbations (left) are generated from 3 different sampling schemes as detailed above. Mean shifts from double perturbations (right) are generated from 4 different sampling schemes. Overall, $(3 + 4) * 10$ shifts are visualized for ID and OOD.

this, both models are equipped with a decoder input dimension that fits the dimensionality of observations. On each noise level, we run 8 trials of random search for both methods. For CPA, we tune the set of parameters described in § 7. For PDAE, we tune the reconstruction loss weight λ , the level of decoder noise and the learning rate. For both methods, the model with the lowest MMD on 7 ID validation environments is selected. Both PDAE and CPA models are then trained for 2000 epochs and evaluated on 7 ID test environments. One random seed is used and shared across data generation, model initialization, training, and evaluation. The results are summarised in Fig. 7. As can be seen, PDAE outperforms the other methods across low and moderate levels of σ_ϵ and converges to the performance of Linear Regression at higher levels of noise. As σ_ϵ grows large, most signal is lost, and the performance of all methods tends to that of the pooling baseline, as expected.

D.3 Details on validation and test cases

For every random seed, we randomly generate 14 ID and OOD perturbation labels. From the fixed training perturbations and the random ID and OOD perturbations, we then generate the two-dimensional latents and corresponding observations. The 14 ID perturbation labels are then split into 7 validation labels used for model selection (hyperparameter tuning) and 7 test labels to evaluate performance. An example of the resulting ground truth distributions for all synthetic train and test cases is visualized in Fig. 9.

Random sampling of test cases. To make the choice of perturbation labels for validation and testing purposes less arbitrary, we set up a random sampling scheme. We propose two separate schemes for generating ID and OOD perturbation labels since their corresponding mean shifts lie within disjoint regions of the Euclidean plane, as shown in Fig. 8a. The ID region of mean shifts is constrained by our training perturbation labels a_0, \dots, a_3 . Together with the elementary mean shifts w_1, w_2, w_3 , i.e., the columns of the perturbation matrix W , the columns of WA constitute the vertices of the unit square as depicted in Fig. 8a. For ease of visualization, we choose the square in the first quadrant with origin at $[0, 0]$ and edge length of 2 to constrain the region of OOD mean shifts. We now explain how the ID and OOD perturbation labels are sampled such that the corresponding mean shifts adhere to the ID and OOD region, respectively.

Single perturbation labels like our training labels only contain one non-zero entry. We therefore sample uniformly from

$$\mathcal{R}_{\text{single}}^{\text{ID}} = \left\{ (a, 0, 0) : a \in [0, 1] \right\} \cup \left\{ (0, b, 0) : b \in [0, 1] \right\} \cup \left\{ (0, 0, c) : c \in [0, 1] \right\} \quad (\text{D.1})$$

For the OOD single perturbation labels, the the non-zero entries lie in $[1, 2]$

$$\mathcal{R}_{\text{single}}^{\text{OOD}} = \left\{ (a, 0, 0) : a \in [1, 2] \right\} \cup \left\{ (0, b, 0) : b \in [1, 2] \right\} \cup \left\{ (0, 0, c) : c \in [1, 2] \right\} \quad (\text{D.2})$$

Similarly, to generate double perturbations from the ID region, we draw uniformly from

$$\mathcal{R}_{\text{double}}^{\text{ID}} = \left\{ [a, b, 0] : a, b \in [0, 1] \right\} \cup \left\{ [a, 0, c] : c \in [0, 1], a \in [0, 1 - c] \right\} \cup \left\{ [0, b, c] : c \in [0, 1], b \in [0, 1 - c] \right\} \quad (\text{D.3})$$

where the restriction to $[1 - c]$ ensures that shifts remain within the ID region.

To create OOD double perturbation labels that imply admissible mean shifts, we define

$$\mathcal{R}_1 = \left\{ [a, b, 0] : a \in [0, 2], b_0 \in [0, 1], b = \mathbf{1}_{\{a \geq 1\}} 2b_0 + \mathbf{1}_{\{a < 1\}} (b_0 + 1) \right\} \quad (\text{D.4})$$

$$\mathcal{R}_2 = \left\{ [a, b, 0] : b \in [0, 2], a_0 \in [0, 1], a = \mathbf{1}_{\{b \geq 1\}} 2a_0 + \mathbf{1}_{\{b < 1\}} (a_0 + 1) \right\} \quad (\text{D.5})$$

$$\mathcal{R}_3 = \left\{ [a, 0, c] : c \in [0, 2], a_0 \in [0, 1], a = a_0(2 - \max(1, c)) + \max(1 - c, 0) \right\} \quad (\text{D.6})$$

$$\mathcal{R}_4 = \left\{ [0, b, c] : c \in [0, 2], b_0 \in [0, 1], b = b_0(2 - \max(1, c)) + \max(1 - c, 0) \right\} \quad (\text{D.7})$$

and then draw uniformly from

$$\mathcal{R}_{\text{double}}^{\text{OOD}} = \mathcal{R}_1 \cup \mathcal{R}_2 \cup \mathcal{R}_3 \cup \mathcal{R}_4. \quad (\text{D.8})$$

We visualize the effects of 70 generated ID and 70 OOD perturbation labels as mean shifts of base state latents in Fig. 8b, i.e., we visualize $\mu_e^z = \mathbf{W}a_e$ for $e \in \{1, \dots, 140\}$.

The number of perturbation labels is chosen as a multiple of 7 since we construct 3 single and 4 double perturbation settings for ID and OOD.

The implied mean shifts for the 4 training, 7 generated ID validation, 7 generated ID test and 14 generated OOD test environments is visualized in Fig. 9.

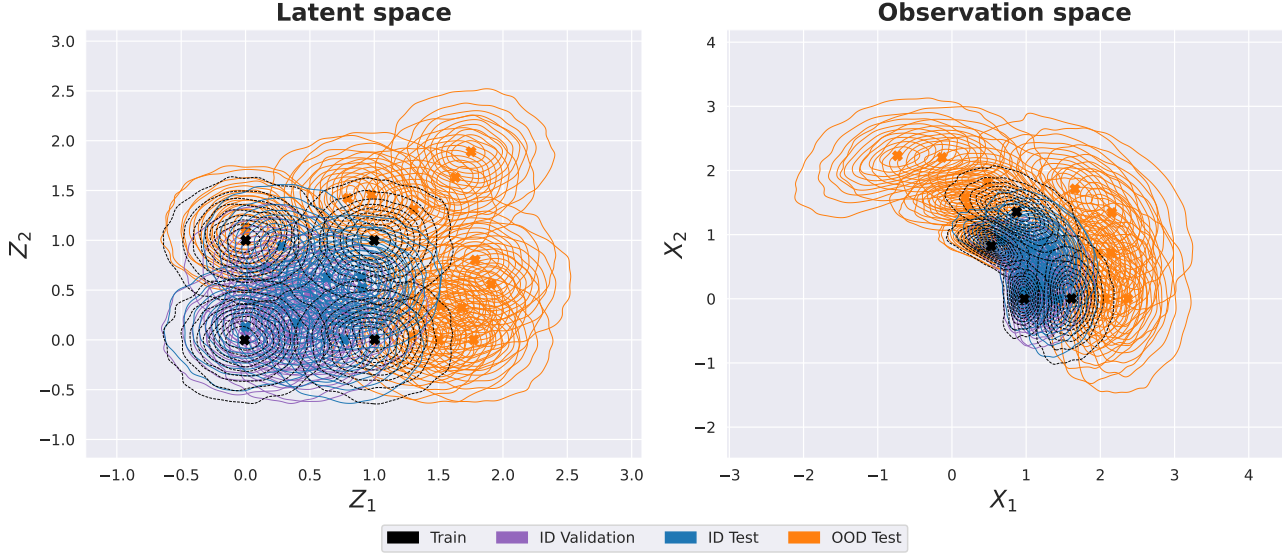


Figure 9. Fixed train environments and randomly sampled validation and test environments with continuous perturbation labels
 We visualize the Kernel Density Estimates of the ground truth distribution of the 4 fixed training environments as well as the randomly sampled 14 ID and 14 OOD environments. The ID environments are split into 7 for validation and 7 for testing. The means of the distributions are visualized with crosses.